Cement and Concrete Research 41 (2011) 477–495

Contents lists available at ScienceDirect

Cement and Concrete Research

journal homepage: http://ees.elsevier.com/CEMCON/default.asp

Improving the structural consistency of C-S-H solid solution thermodynamic models

Dmitrii A. Kulik *

Paul Scherrer Institut, Laboratory for Waste Management, 5232 Villigen PSI, Switzerland

ARTICLE INFO

Article history:
Received 16 September 2010
Accepted 19 January 2011

Keywords:
Calcium-silicate-hydrate (C-S-H) (B)
Thermodynamic calculations (B)
Modelling (E)
Solid solutions (B,E)
Aqueous solubility (B)

ABSTRACT

Simple aqueous–solid solution models of C-S-H (calcium silicate hydrate) are widely used in studies of cement hydration and waste–cement interactions. Even without a clear structural/mechanistic basis, such thermodynamic models yield a good description of solubility data in [Ca]-C/S space, while only satisfactory in [Si]-C/S, H_2O-C/S, [Ca]–[Si] spaces and in the $0.1<C/S<0.8$ range. Here, using a multi-site (sublattice) concept, the ideal solid solution model of C-S-H is revised to make it consistent with the Richardson–Groves structural model of C-S-H and with the modern interpretation of spectroscopic (^{29}Si MAS NMR) and solubility data. Consideration of two site substitutions, (1) coupled H_2OCa^{2+} for $SiO_2H_2^{2+}$ replacement in bridging tetrahedral and adjacent interlayer sites, and (2) substitution of interstitial $Ca(OH)_2$ for a vacancy, leads to a new CSHQ model of (A,B) (C,D)X type composed of two tobermorite-like and two jennite-like end members. Because this ideal sublattice SS model cannot fit solubility data well at $0.8<C/S<1.1$, a simpler CSH3T model is constructed from a polymeric TobH $(CaO)_2(SiO_2)_3(H_2O)_5$, a dimeric T2C $(CaO)_3(SiO_2)_2(H_2O)_5$, and an ordered pentameric T5C $(CaO)_{2.5}(SiO_2)_{2.5}(H_2O)_5$ tobermorite-like end members. This solid solution model, limited to the range $0.67<C/S<1.5$, has a correct built-in dependence of the mean silicate chain length on C/S, yields quite realistic fits to the solubility data, and provides a basis for extensions with foreign cations whose sites in the defect-tobermorite structure of C-S-H are known. To account for C-S-H compositions with $C/S>1.5$, CSHQ end members were downscaled to one tetrahedral site and used within the simple mixing model. Despite some loss of structural consistency, the solubility and mean silicate chain length data can be reproduced well with this downscaled CSHQ model, capable of temperature corrections and dependencies of density and water content in fully-hydrated C-S-H on C/S ratio. Most literature solubility data sets can be modeled at the cost of moderate adjustments of CSHQ end-member solubility products within 0.2 to 0.6 pK units.

1. Introduction

Knowledge of the solubility and stability of calcium silicate hydrates (C-S-H) is important because the C-S-H formation and structure determine hardening process and strength of cement, and play the major role in cement degradation [1]. Ubiquitous C-S-H gel-like phase is the main sorbent for Na, K and hazardous cations in hydrated cements used in engineered barriers of (nuclear) waste repositories [1–6].

C-S-H has variable composition and shows an incongruent solubility upon de-calcification, re-calcification, carbonation and

Abbreviations: Aq-SS, Aqueous solid solution (model); BT, Bridging tetrahedral site (in sublattice C-S-H models); BTI, Bridging tetrahedral interlayer combined site (in simplified sublattice models); C curve, Solubility [Ca]–[Si] eye-guide curve for C_3S hydration samples [18]; C" curve, Solubility [Ca]–[Si] curve for double-decomposition C-S-H samples [18]; C3S, Tricalcium silicate, Ca_3SiO_5; CEF, Compound energy formalism (based on the sublattice concept); CH, Portlandite, $Ca(OH)_2$; CL, Chain length (of silica 'dreierketten'); <CL>, mean chain length; C-S-H, Calcium silicate hydrate (gel-like phase); CSH3T, Ternary solid solution model for C-S-H of tobermorite-like structure; CSHQ, Quaternary solid solution model for C-S-H of tobermorite–jennite-like structure; CU, Calcium hydroxide unit (in sublattice models); C/S, Calcium to silicon (mole ratio in the solid part of the system); GEM, Gibbs energy minimization; GEMS, GEM-Selektor geochemical modeling package (http://gems.web.psi.ch); H/S, H_2O to SiO_2 (molar) ratio in bulk solid; IC, Interlayer cation site (in sublattice models); IW, Interlayer water site (in sublattice models); J2, Dimeric half-protonated jennite-like end member; J2C, Dimeric jennite-like end member with full interlayer Ca^{2+} occupancy; JenH, Jennite-like end member with H^+ (without Ca^{2+}) in the interlayer; LDH, Layered double hydroxide; MAL, Mass-action law; MAS, Magic angle spinning; NMR, Nuclear magnetic resonance; RG, Richardson and Groves' (structural model of C-S-H); RH, Relative humidity (in percent for a given temperature); SH, Amorphous hydrous silica SiO_2 phase; SS, Solid solution; T2, Dimeric half-protonated tobermorite-like end member; T2C, Dimeric tobermorite-like end member with full interlayer Ca^{2+} occupancy; T5C, Pentameric tobermorite-like end member with full interlayer Ca^{2+} occupancy; T/CH, Tobermorite/Interstitial calcium hydroxide (structural concept); T/J, Tobermorite/Jennite (structural concept); TGA, Thermogravimetric analysis; TU, Tobermorite (structural calcium silicate) unit (in sublattice models); TobH, Tobermorite-like end member with H^+ (without Ca^{2+}) in the interlayer; V_{CH}, Vacancy (of CH on the CU sublattice site), similarly V_{BT}, V_{IW}; XAS, X-ray absorption spectroscopy; XPS, X-ray photoelectron spectroscopy; XRD, X-ray diffraction; [M], Total molarity of aqueous dissolved ionic M (mol dm^{-3}).

* Tel.: +41 56 3104742; fax: +41 56 3102821.
E-mail address: dmitrii.kulik@psi.ch.

0008-8846/$ – see front matter © 2011 Elsevier Ltd. All rights reserved.
doi:10.1016/j.cemconres.2011.01.012

Nomenclature

A_γ	Debye–Huckel parameter (in Davies equation)
Cp^o	Standard isobaric heat capacity (in J K^{-1} mol^{-1})
H^o	Standard enthalpy (in J mol^{-1})
G_f^o	Standard Gibbs energy function of (end member) compound, in J mol^{-1}
I	Effective ionic strength of aqueous electrolyte (molal)
Q	Number ratio of singly-bonded silica tetrahedra to all silica tetrahedra (<Q> is the mean ratio)
P	Pressure (bar)
R	Universal gas constant (8.31451 J K^{-1} mol^{-1})
S^o	Absolute entropy at standard state (in J K^{-1} mol^{-1})
T, T_r	Temperature (K), reference temperature $T_r = 298.15$ K
V^o	Standard molar volume (in J bar^{-1})
Z_j	Formula charge of j-th aqueous ionic species
a_j	Thermodynamic activity (of j-th solid solution end member)
c	Basal distance parameter (of tobermorite-like structure)
h	H_2O content stoichiometry coefficient ($0.4<h<2$)
m	Number of H_2O molecules bound but not present as hydroxyls (in RG model)
n	Number of 'dreierkette' units in silicate chain of length $CL = 3n - 1$ (RG model)
n_{Si}	Factor for scaling the bulk formulae of C-S-H SS end members
w/n	Degree of protonation of silanol groups (RG model)
u	Degree of protonation of silanol groups (re-normalized RG model), $u = w/n$
v	Number of vacant tetrahedral sites per silica 'dreierkette', $v = 1/n$ (<v> average)
x_j	Mole fraction of j-th solid solution end member
y	Number of Ca^{2+} cations compensating permanent charge or present as extra CH units (in RG model)
y_i	Site fraction of i-th substituting species on a sublattice site
ΔG_{ord}	Standard Gibbs energy effect of the ordering reaction between end members
ΔG_{rcp}	Standard Gibbs energy effect of the reciprocal reaction between end members
γ_j	Activity coefficient of j-th aqueous species (Davies equation)
λ_j	Activity coefficient of j-th end member (also fictive activity coefficient $\lambda_j = a_j/x_j$)
μ_j	Chemical potential of j-th end member (J mol^{-1})
ρ	Density (in g cm^{-3}), ρ_{sat} in water-saturated system

dilution in a region $0.7<C/S<1.7$ when no portlandite (CH) or hydrous silica (SH) phases are present [1]. C/S denotes here the mole ratio of CaO to SiO_2 in the solid part of the system. The water content in C-S-H is usually expressed as C/S + h, where $0.4<h<2$ depending on the relative humidity and other factors [7–9]. Dissolved total silicon [Si] and calcium [Ca] molar concentrations vary with C/S and deviate from it everywhere, except a narrow 'congruence region' $0.8<C/S<0.9$. Above this region, re-calcification causes a rapid transformation of C-S-H into C-S-H with higher C/S, whereas de-calcification, carbonation, or dilution result in an inverse process. This can be modeled using one or two C-S-H solid solutions (SS) in equilibrium with other hydrated cement phases and aqueous electrolyte.

Existing thermodynamic models of C-S-H solubility range from purely empirical fits to complex non-ideal SS models, and describe the experimental data from satisfactory to good. Our simple ideal two-SS-phase model of C-S-H [10] has been used in modeling cement hydration [11–13], and later incorporated into the Cemdata-07 data base [14] (http://www.empa.ch/cemdata), a plug-in for the GEM-Selektor geochemical modeling package (http://gems.web.psi.ch). This SS model describes well the total dissolved calcium [Ca] and pH as functions of C/S, but only satisfactory reproduces [Si] versus C/S and the C-S-H solubility in [Ca]–[Si] coordinates. Other shortages include the lack of verification with structural/spectroscopic data, and the questioned existence of CSH-I SS phase acting at $0<C/S<0.8$.

During the last 10–12 years, a lot of crystallographic and spectroscopic information on C-S-H and its structural analogs, tobermorite and jennite, has been collected [15–23]. This data corroborates structural models of C-S-H suggested by Taylor [24–26], Richardson and Groves [19,27], as well as the "defect tobermorite" model [28,29]. A deep insight into the structural evolution of C-S-H in response to re/de-calcification and conditions of preparation is presented in [18]. Accurate modeling of variable-composition solids requires the solid solution model at best be derived from the atomistic arrangements.

The main goal of the present contribution was to employ structural insights for revising and improving the accuracy and plausibility of our thermodynamic C-S-H ideal SS model [10,11,13]. In doing this, the *sublattice site concept* has been used in determining the number and stoichiometry of end members and verifying them with solubility data and structural information, such as the mean silica chain length <CL> measurable e.g. with ^{29}Si MAS NMR spectroscopy. Another goal was to make the SS model more plausible in reproducing the water content and density of C-S-H (at 100% relative humidity). In turn, achievement of these goals should make thermodynamic models of cement hydration and of chemical degradation of cement matrix with sorbed foreign cations more useful.

Keeping the C-S-H SS model as simple as possible is crucial for the ease of its extension to the sorption of minor cations in C-S-H — as an alternative to ion-exchange models used in studies related to waste management. The alternative, surface complexation model setup, is justified when the emphasis is put on the surface charging and cohesion of C-S-H particles ([30–32]), but this issue is beyond the scope of the present paper.

In Section 2 of the following text, a brief overview of C-S-H structural models, solubility, density, water content, and previous thermodynamic modeling approaches are provided. A new, more structurally consistent definition of the ideal sublattice solid solution model of C-S-H is described in Section 3 (with some didactic details collected in Appendix A); this includes a conversion of the RG structural model into a form, which is suitable for defining sublattices and substituting species on structural sites. Details of GEM-Selektor thermodynamic calculations (with supporting thermodynamic data in Appendix B) and parameterization of C-S-H solid solution models are given in Section 4, first for the simplified ternary CSH3T model limited to tobermorite-like structure and $C/S<1.5$, then for the downscaled quaternary CSHQ model related to both tobermorite- and jennite-like structures in the C/S range from 0.67 to 2.25. The sensitivity study of the capability of downscaled CSHQ model to describe various metastable C-S-H phases represented by several published solubility data sets is described in the Supporting Information file. Finally, the Section 5 contains the discussion of new C-S-H solid solution models and to what extent their structural consistency has been improved.

2. C-S-H structure, solubility, and previous solid solution models

2.1. Structural models of C-S-H

Existing structural models of C-S-H were recently compared by Richardson [20] who concluded that there is more of a consensus than it might seem. The models fall into two groups: (1) where the silicate anions are entirely monomeric, and (2) those derived from the dreierkette-type of silicate chain present in the 1.4-nm tobermorite.

None of the monomer-based models are consistent with the experimentally observed distribution of silicate anions in C-S-H formed already after the short induction period of C3S hydration. The dreierkette-based models, corroborated with TMS data, ^{29}Si MAS NMR, XAS, XRD, Raman, and XPS spectroscopies, describe such distribution mainly by assuming the removal of some dreierkette bridging tetrahedra along with the exchange of Ca^{2+} ions. Whereas the dreierkette-based models may seem quite different (see Table 2 in [20]), they are, in fact, quite similar, and may be considered as special cases of the structural model suggested by Richardson and Groves [19,27,33]. Their model can be interpreted from either tobermorite/jennite (T/J) or tobermorite/interstitial $Ca(OH)_2$ (T/CH) structural viewpoints; it also allows for the incorporation of cations and anions other than Ca^{2+}, H^+, SiO_3^{2-} and OH^- by defining more structural substitutions.

The Richardson–Groves' (RG) structural model is expressed as [19]:

$$[Ca_{2n}H_wSi_{(3n-1)}O_{(9n-2)}]\cdot(OH)_{w+n(y-2)}\cdot Ca_{(n\cdot y)/2}\cdot mH_2O \quad (1)$$

where: m is the number of water molecules bound but not present as hydroxyl groups; $n = 1,2,\ldots,\infty$ is the number of *dreierkette units* in the silicate chain of length $CL = 3n-1$; w/n is the degree of protonation of silanol groups; and y is the number of Ca^{2+} cations compensating the remaining permanent charge or present as extra $Ca(OH)_2$. These parameters are constrained as:

$$\begin{array}{ll} \text{for } 0\le y\le 2,\ n(2-y)\le w\le 2n & (\text{T}-\text{units});\\ 2\le y\le 4,\ 0\le w\le 2n; & \\ 4\le y\le 6,\ 0\le w\le n(6-y) & (\text{J}-\text{orCH}-\text{units}). \end{array} \quad (2)$$

The C/S ratio is given by

$$C/S = \frac{n(4+y)}{2(3n-1)}. \quad (3)$$

Deviations from C/S = 5/6 (theoretical value for 1.4 nm tobermorite taken as a structural prototype of C-S-H) can result [19] from:

(i) Omission of bridging tetrahedra, with a decrease in mean <CL> and increase in C/S;
(ii) Change in the content of Ca^{2+} ions balanced by the opposite change of Si–OH groups, manifested by variations $2\le w/n\le 0$ and $0\le y\le 2$, and respectively by the C/S ratio;
(iii) Incorporation of additional $Ca(OH)_2$ moieties reflected in an increase in y from 2 to 4, leading to an increase in C/S ratio.

Structural modifications (i) and (ii) apply to both T- or to J-units. In the T/J view, modification (iii) is the transition from T- to J-structural units; in the T/CH view, this involves the incorporation of interstitial CH layers. The ranges in Eq. (2) define a compositional space for C-S-H, in which the ranges $2/3\le C/S\le 1.5$ for the T structure and $4/3\le C/S\le 2.5$ for the J structure overlap in the intermediate 'mixed T/J' composition range at $1.0\le C/S\le 2.0$ [19].

Taylor's T/J structural model of C-S-H [26] can be obtained from the RG model as a special case by setting $w = n$ ($w/n = 1$) and substituting $y = 1$ for T units and $y = 5$ for J units in Eq. (1) (see Ref. [19] p. 1766). Thus, the C-S-H structure is assumed to have a medium level of protonation of silanol groups (one per three tetrahedral sites or dreierkette unit) at any composition.

The Cong–Kirkpatrick defect-tobermorite model [28] corresponds to a RG model sub-space with $y = 2$ and $w/n = 0$ for the case when all silanol groups are balanced with Ca^{2+} cations; there is some variability when either w/n increases and y decreases, or both w/n and y increase (details in Ref. [19] p. 1766).

The defect-tobermorite model proposed by Nonat and Lecoq [30,34] as their 'first hypothesis' corresponds to the RG model with $w/n = 0$ and $y = 2$. Their 'second hypothesis' implies the presence of OH^- and Ca^{2+} ions in the interlayer space, similar to the early Stade–Müller model ([35] and refs. therein), but differs from the RG model in that Si-O-Ca-OH linkages involve the interlayer Ca rather than the main-layer Ca.

Chen et al. [18] interpreted C-S-H solubility and structure using arguments not really much different from those in the T/J view of RG model. Charge-balance calculations [18], aimed at determining a C/S ratio above which the –Ca–OH moieties must be present in C-S-H, all correspond to T-units with $w/n = 0$ and $y = 2$, the same as in the Nonat's 'first hypothesis' or in the 'balanced' Cong–Kirkpatrick defect-tobermorite model. However, Chen et al. [18] provide more data and arguments that are helpful to simplify solid solution models of C-S-H in the context of the present contribution.

Recently, for a mechanochemically synthesized nanocrystalline C-S-H (I) SS phase, Garbev et al. [22,36] presented a structural model backed up by Raman, synchrotron-based XRD, ^{29}Si NMR, XPS and TGA studies. They tend to corroborate the early model by Stade and Wieker [37], and point to the existence of two well-ordered end members — one with C/S = 2/3, basal distance $c = 1.33$ nm, and another with C/S = 5/4, $c = 1.17$ nm. The former has the structure very similar to that of 1.4 nm tobermorite, but without the interlayer calcium, and with T-layers assumed to hold together via the network of hydrogen bonds. The latter is essentially a tobermorite-based dimer with all bridging tetrahedra missing and with T-layers connected by the interlayer Ca^{2+} ions. 'Mixing' between these end members corresponds to the defect-tobermorite model, in which variations in C/S ratio are explained by two competing mechanisms: (1) variation in the interlayer Ca content, and (2) omission of bridging silicate tetrahedra. In terms of the RG model (Eq. (1)), the first end member has $n = \infty$ and $w/n = 2$, while the second end member has $n = 1$ and $w/n = 1$. Based on the TGA data, Garbev et al. [22] found the maximum non-hydroxyl water content of $4H_2O$ in the C/S = 5/4 end member and in C-S-H with C/S = 1, and $3.3H_2O$ in the C/S = 2/3 end member (expressed here per three tetrahedral sites).

In their series of nanocrystalline C-S-H(I) samples, Garbev et al. [36] observed rather constant basal c-distances about 1.33 nm at target C/S from 1/5 to 3/4, rather constant c about 1.17 nm at C/S from 6/5 to 3/2, and a rather sharp transition between C/S = 0.8 and 1.1. They interpreted this as an indication of a possible miscibility gap at C/S between 5/6 and 1/1, inside of a disordered series within the range $2/3 < C/S < 4/3$; however, they did not provide any solubility data for checking this assumption. The intermediate structure at C/S = 1/1 was considered as having $<CL> \approx 5$ and a stronger ordering. The presence of portlandite in samples with target C/S of 4/3 and 3/2 was explained by the exsolution of additional portlandite slabs by the mechanochemical treatment, which seems to prevent the formation of jennite-like structures.

From structural arguments and spectroscopic data, two to three C-S-H SS phases are assumed to exist at $2/3 < C/S < 2$, termed either C-S-H(I) and (II), or α-, β-, γ-C-S-H [30]. However, the evidence for two SS phase regions on C-S-H solubility diagrams is not convincing; most solubility data sets do not show a clear inflection or "shelf" around C/S = 1 that, if present, would indicate a 'miscibility gap', i.e. co-existence of two C-S-H phases of different composition. This 'simple' behavior may be attributed to globular aggregates of tobermorite-like or jennite-like nano-domains with relatively high specific surface area ([38] and refs therein), which comprise most of C-S-H samples prepared by co-precipitation or C3S hydration. Both particle size effect on solubility and sorption of extra calcium on outer surfaces or edges of nano-domains may result in apparently simple C-S-H solubility curves.

Overall, the shortage of almost all structural models of C-S-H phases lies in their weak connection with the stability and solubility data. No estimates of relative stabilities of structurally derived end member compounds were provided in the RG and related models. Work by Chen et al. [18] is notably exceptional in relating solubility and structural (spectroscopic) studies for the same series of C-S-H samples and elucidating the extent of reversibility of C-S-H properties

upon de/re-calcification. However, even this work did not advance that far as to model the whole C-S-H aqueous–solid solution system in a thermodynamically sound way.

2.2. C-S-H solubility, water content, and density

C-S-H solubility at room temperature has been studied over decades [4,8,18,39–48]. C-S-H samples with different C/S ratios were prepared by (controlled) C3S or C2S hydration, or by co-precipitation methods, with the subsequent curing time from days to months (see Table 1 in Ref. [46]). Most of the earlier data was summarized by Berner [49,50] in a first attempt to model the incongruent solubility of C-S-H. Chen et al. [18] considered C-S-H solubility as function of C/S ratio in the light of available ^{29}Si MAS NMR data and charge balances, also using the Jennings' [51] diagram where the C-S-H solubility is rendered in [Ca]-log[Si] space along a family of eye-guide curves. Different curves (A, C″, C′, C) were related to the method of synthesis, to the content of −Ca–OH, and to the extent of silicate polymerization in C-S-H. According to Chen et al. [18], the observed solubility differences arise from systematic variations in C/S, silicate structure, and −Ca–OH content in a spectrum of metastable phases, structurally ranging from purely tobermorite-like (Curve A) to largely jennite-like (Curve C).

The water content and density of C-S-H were recently re-evaluated by Brouwers [9]. For the clinker hydration product (aged 126 days or longer) with C/S = 1.7, the content of non-evaporable water was estimated as $C_{1.7}SH_{1.2}$ at the density $\rho = 2.86$ g cm^{-3}. The content of water in saturated state (at 100% RH) was found to be $C_{1.7}SH_{3.2}$ at the density $\rho_{sat} = 2.25$ g cm^{-3}. Assessments were also made for C-S-H with C/S ≠ 1.7 using two alternative concepts: (1) constant gel water, or constant density; (2) variable gel water, with density increasing as C/S decreases (see Fig. 6 in Ref. [9]). Case (1) leads to C_xSH_{x+h} stoichiometry in the whole C/S range, with constant h = 0.8 [8,39], and h = 1.7 [7] or h = 2.0 [9] in saturated state. Case (2) is based on experiments by Lu et al. [52] who found that the amount of gel water decreased with a decrease in C/S from 1.6 to 1.2; at C/S = 1.2, that amount decreased with aging time, tending to $C_{1.2}SH_{1.6}$. The variable gel water case can be represented as $C_xSH_{3x-1.9}$ [9], but at C/S < 1.0 this stoichiometry yields the unrealistically high density (>2.8 g cm^{-3}).

The findings [22] about lower water content and decreased *c* distance in dimeric nanocrystalline C-S-H seem to corroborate the case (2) at C/S > 1.25, adding to it a trend of decreasing density with decreasing C/S at C/S < 1.25. Hence, in the saturated state, the formula $C_xSH_{3x-1.9}$ must be limited to C/S > 1.25, and replaced with $C_xSH_{0.6+1.25x}$ at C/S ≤ 1.25. The density maximum at C/S = 1.25 will be ca. $\rho = 2.5$ g cm^{-3}, and the density at C/S = 0.7 is ca. $\rho = 2.2$ g cm^{-3}.

2.3. Previous approaches to model solubility of aged C-S-H phases

The C-S-H solubility has been modeled using MAL speciation codes [46,48,49,53], as well as GEM phase equilibrium solvers [10,11,54–56]. The MAL (mass action law) method, implemented in programs such as PHREEQC, uses input thermodynamic data in the form of equilibrium constants K^o of formation reactions for product species (aqueous complexes, exchange ions, minerals, SS end members). The GEM (Gibbs energy minimization) is used in the Calphad software (e.g. Thermo-Calc [57]), as well as in geochemical modeling codes such as the GEM-Selektor (http://gems.web.psi.ch). The input thermodynamic data in GEM is the standard molar Gibbs energy function G_f^o (corrected to the temperature of interest) for all components in all phases. A detailed comparison of methods and codes is given in [58]. GEM is suitable for modeling equilibria with simultaneous aqueous electrolyte, gas/fluid mixture, and several multi-component (non-)ideal solid solutions, plus many pure condensed phases [57,58].

In the MAL approach, C-S-H solubility was first simulated using the solubility products of pure SiO_2, CaH_2SiO_4, $Ca(OH)_2$, … solids, varying as empirical functions of C/S ratio in the C-S-H gel [49,53,59]. Such functions of C/S ratio were also derived using a non-ideal binary solid solution model with end members SiO_2 and $Ca(OH)_2$ [48]. In a Lippmann diagram approach, a non-ideal binary SS between "tobermorite" and $Ca(OH)_2$ was considered [46,48,60,61] without- or with MAL speciation calculations. Note that the high non-ideality in such C-S-H SS models may be due to using $Ca(OH)_2$ instead of a structurally more realistic C-S-H end member with C/S ≤ 2.

A thermodynamically sound model of equilibrium in the CaO-SiO_2-H_2O system was implemented by Thomas and Jennings [55] using the commercial Thermo-Calc software. The available structural and NMR data for the defect-tobermorite model [28] were translated into a C-S-H solid solution model with five sublattices expressed as:

$$[CaO]:_{2.33}\left[Ca^{2+}, H_2^{2+}\right]:_{1.0}[SiO_2]:_{2.0}\left[H_2SiO_4^{2-}, H_2O_2^{2-}\right]:_{1.0}[H_2O]_{5.0}$$

where the colons separate different sublattices (i.e. sets of structurally equivalent sites), and the numbers below are site stoichiometry ratios [55]. The model assumes two independent, charge-balanced substitutions in the second and in the fourth sublattices, yielding four end members with C/S ratios of 1.11; 1.67; 0.78; and 1.165 (covering the range 0.78 < C/S < 1.67). The fourth sublattice has been chosen consistently with the observed $Q = 0.7$ at C/S = 1.5 (here, the parameter Q is a number ratio of singly-bonded silica tetrahedra Q1 to all silica tetrahedra Q2, Q3,…; $Q = 1$ when only dimers are present). Assuming the ideal mixing in each sublattice, the G_f^o values of end members were fitted from a single experimental point at C/S = 1.34, [Ca] = 10 mM, [Si] = 12 μM, and $Q = 0.585$. This ideal solid solution model described well the lower curve on Jennings' diagram [51], but deviated in reproducing the Q parameter. Next, the excess subregular interaction parameters were introduced for both Ca^{2+}–$2H^+$ and $H_2SiO_4^{2-}$–$H_2O_2^{2-}$ substitutions, and the model was refitted using up to 30 data points. This led to a much less stable end member with C/S = 1.165 and large negative interaction parameters for the substitution in second sublattice.

So far, the structurally reasonable quaternary non-ideal solid solution model [55] has not been much in use, perhaps because it needs the expensive Calphad software with undisclosed thermodynamic data base, precluding its implementation in open geochemical GEM or MAL codes. Recently, the sublattice solid solution model of C-S-H has been re-implemented for a 25 to 85 °C temperature interval [56] using the MTDATA code (another piece of Calphad software). Unfortunately, the authors [56] did not explain how they derived sublattices and end members, did not account for charge balance, and did not provide the standard molar Gibbs energies for end members, which again renders their model not reproducible in other codes.

The simple ideal mixing between tobermorite-type and jennite-type end members was a main assumption behind the C-S-H solid solution model by Sinitsyn et al. [54], later on elaborated in Refs. [10,11] and included into the Cemdata'07 data base (http://www.empa.ch/cemdata) [13]. This simple model, originally used with GEM codes (e.g. GEM-Selektor), can also be calculated using the PHREEQC code [62]. In CO_2-free system (Ca-H-O-Si-e), the whole model includes four phases: aqueous electrolyte Aq, portlandite CH, low-Ca C-S-H CSH-I, and high-Ca C-S-H CSH-II. The CSH-I phase is assumed to be a simple ideal solid solution between SH (amorphous hydrous silica) and Tob-I (tobermorite-like, C/S = 5/6) end members. The CSH-II phase is a simple ideal solid solution between Tob-II (C/S = 5/6) and Jen (jennite-like, C/S = 5/3) end members. Both phases co-exist in a narrow interval 0.8 < C/S < 0.9; the CSH-II phase co-exists with the CH (portlandite) phase at C/S > 1.6.

Because non-ideal excess energy parameters have not been used in this model, the only possibility to fit it to the experimental solubility data was to adjust the molar G_f^o values of end members while, if necessary, re-scaling their stoichiometry [10]. In this semi-empirical way, a good fit to a particular solubility data set can be achieved; Kulik and Kersten [10] explain this on the basis of sublattice- and interstitial

Table 1
CSH-I – CSH-II SS model [10]: Cemdata'07 [13] version, and its 'adjusted' variant.

End-member	Stoichiometry	C-S-H SS model [13]		Adjusted to data [41]	
		n_{Si}	G_f^o	n_{Si}	G_f^o
SH-I	$[SiO_2]_{nSi}$	1	−848.90	1	−848.90
Tob-I	$[(CaO)_{0.83}(SiO_2)_1(H_2O)_{1.33}]_{nSi}$	2.4	−4186.45	2.4	−4370.30
Tob-II	$[(CaO)_{0.83}(SiO_2)_1(H_2O)_{1.33}]_{nSi}$	1	−1744.36	1.8	−3277.72
Jen-II	$[(CaO)_{1.67}(SiO_2)_1(H_2O)_{2.1}]_{nSi}$	1	−2480.81	0.9	−2353.32

G_f^o values are given in kJ mol^{-1} for $P=1$ bar, $T_r=298.15$ K; n_{Si} is the stoichiometry scaling factor.

solution concepts [63], as also exemplified in ([58] p. 40–44). It follows that re-scaling of end members is justified, if substitutions that alter C/S ratio and stability of C-S-H phase occur mainly in one sublattice. A very reasonable fit of the model [10] to the C-S-H solubility data [41] ([Ca] and pH vs C/S in solid) shows that this idea may not be wrong (Table 1 and Fig.1).

A decade of using the aqueous two-solid-solution model of C-S-H has been sufficient to reveal its strengths and weaknesses. The unclear mechanistic background is now seen as a drawback and a possible reason of [Si] over-prediction both in [Si]-C/S and [Si]–[Ca] spaces. The lack of an internal degree of freedom is manifested by a much worse model fit to [Si] data after improving the fit to [Ca] (see dashed curves on Fig. 1 that correspond to the "Adjusted to data [41]" numbers in Table 1). It is difficult, if ever possible, to obtain with this model the good fits simultaneously in [Si]-C/S and [Ca]–[Si] spaces. Hence, a revision of structural background of the C-S-H SS model and re-definition of the number and stoichiometry of end members appears necessary.

3. New formulation of C-S-H solid solution model

The structural information summarized above (Section 2.1) can help improve the C-S-H SS model in several aspects, namely (i) definition of sublattices, interstitions, defects and other structural sites; (ii) elucidation of site occupation and substitution mechanisms; (iii) constraining the compositional ranges and end member stoichiometries; (iv) evaluating configurational entropies and possible non-ideality effects. A closer match between the atomistic structure and the thermodynamic SS model can be achieved using the *sublattice concept* or *compound energy formalism* (CEF) used in metallurgy (e.g. [57,65]), mineralogy and petrology (e.g. [66]).

CEF begins with the definition of *sublattices*, i.e. sets of equivalently coordinated sites (and charges) in the crystal structure [57]. The next step is to consider, which species (atoms, ions or vacancies) can be substituted in a sublattice site. A single species in each sublattice (no substitution) is a trivial case of the pure (stoichiometric) solid phase. Random mixing in a sublattice is described by a configurational entropy $S_{conf} = -R\sum_i y_i \ln y_i$, where y_i is the site fraction of i-th substituting species, and R is the universal gas constant. If there is only one sublattice with two or more substituting species then the S_{conf} expression reduces to that for a simple random mixing of end members, $S_{simple} = -R\sum_j x_j \ln x_j$, where x_j is the j-th end-member mole fraction, $x_j = y_i$, $i=j$. In more complex cases, there may be several sublattices with different substitutions. Usually, it is assumed that the random mixing in

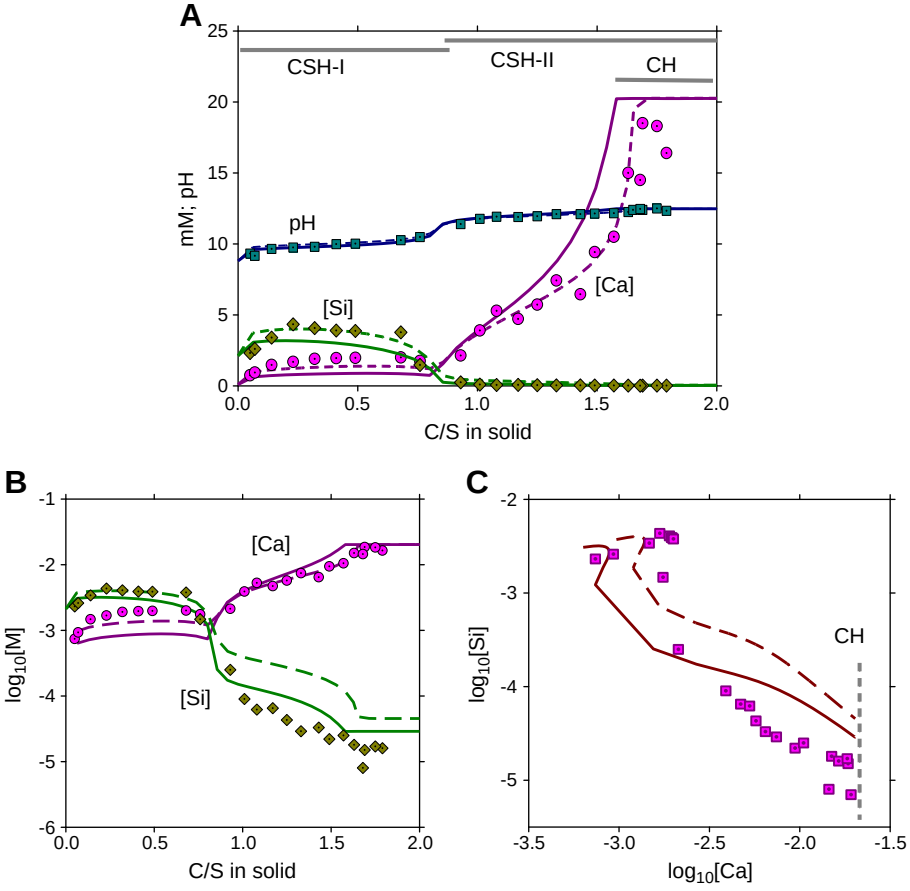

Fig. 1. Solubility diagrams at 1 bar 25 °C, obtained using CSH-I and CSH-II solid solution models from Table 1 (other thermodynamic data from Cemdata'07 data base [13] and Nagra-PSI data base [64], GEMS version). The model variant adjusted to [Ca] data [41] is shown in dashed curves; this variant fits the [Si] data worse. Note reasonable fits to solubility data [41] in [Ca]-C/S and [Si]-C/S spaces (A, B), but larger deviations in the [Ca]–[Si] space (C).

sublattices occurs independently, so the total S_{conf} will be a weighted sum of S_{conf} for each sublattice. For instance, in the $[A,B]_2[C,D]_1$ solid solution system,

$$S_{conf} = -R(2y_A \ln y_A + 2y_B \ln y_B + y_C \ln y_C + y_D \ln y_D)).$$

A list of solid solution end members is created by combining one species per sublattice site (e.g. A_2C, B_2C, A_2D and B_2D in the above example). Since not all such end members may exist in pure state, there is a problem of estimating or fitting their thermodynamic properties [57,65]. The site fraction for i-th species can be represented as a sum of mole fractions of end members that contain this species on this sublattice. In absence of non-ideal (excess) terms, the activity of end member will be equal to a product of site fractions of species that it contains (e.g. for A_2C, $a_{A2C} = y^2_A \cdot y_C$), but not $a_j = x_j$ as in the simple ideal mixing.

Equilibria involving 'multi-site' SS models can be solved only with GEM software. Papers [10,55,56] present first attempts to apply sublattice concepts in part or in full to C-S-H SS systems. The task of the present contribution was to recast the Richardson and Groves [19] structural model into a form suitable for defining sublattices, substitutions, and end members for the revised C-S-H solid solution model.

3.1. Derivation of a sublattice SS model from the RG structural model

Firstly, the RG model has been re-normalized to one dreierkette unit (i.e. three adjacent tetrahedral sites) by dividing Eq. (1) by n:

$$[Ca_2H_uSi_{3-v}O_{9-2v}]\cdot(OH)_{u+y-2}\cdot Ca_{1-u/2}\cdot Ca_{y/2-1+u/2}\cdot mH_2O \quad (4)$$

Now, $u = w/n$ is the extent of protonation of silanol groups, and $v = 1/n$ is the number of vacant tetrahedral sites per silica dreierkette ($0<v<1$). Eq. (3) can now be simplified to

$$C/S = \frac{4+y}{2(3-v)} \quad (5)$$

and the C-S-H composition formula (4) can be re-written as

$$[Ca(OH)_2]_{(u+y-2)/2}\cdot[(CaSiO_{3.5})_2\cdot(SiO_2)_{1-v}]\cdot(H_u\cdot Ca_{1-u/2})\cdot mH_2O \quad (6)$$

where $[Ca(OH)_2]_{(u+y-2)/2}$ represents the 'jennite' or 'interstitial CH' unit; $(H_u\cdot Ca_{1-u/2})$ depicts cation exchange in the interlayer to balance the charge of the dimeric tobermorite structural unit $(CaSiO_{3.5})_2^{2-}$, and $(SiO_2)_{1-v}$ represents silica in the bridging tetrahedral (BT) site. By considering the following limits: 0 to 2 for u, 0 to 1 for v, 0 to 6 for y and 2 to 5 for m, a corresponding sublattice stoichiometry formula can be obtained:

$$\left[IC^+\right]_2 : [TU^-]_2 : \left[BT^0\right]_1 : \left[CU^0\right]_2 : \left[IW^0\right]_5. \quad (7)$$

Each term (separated by colons) corresponds to a sublattice, defined as a set of identical sites in the mineral structure (shown schematically in Fig. 2).

The site occupancies are $u/2$ for H^+ and $1-u/2$ for Ca^{2+} in IC sites; $1-v$ for SiO_2 and v for a vacancy V_{BT} in BT sites; $m/5$ for H_2O and $1-m/5$ for a vacancy V_{IW} in IW sites; and $(u+y-2)/4$ for $Ca(OH)_2$, $1-(u+y-2)/4$ for a vacancy V_{CU} in CU sites. Following the RG model, we assumed that the permanent charge in C-S-H structure is carried by the TU Ca-silicate units and not by the BT site itself. Note that there is no formal difference between J and CH structural viewpoints of the RG model; hence, only the T/J (tobermorite/jennite) nomenclature will be used further on. The stoichiometry ratio of IW (interstitial water) sites can be set to 5 according to the maximum possible water content in C-S-H.

This model has nominally 4 sublattice site types, each with 2 substituting species, resulting in 16 end members. Equilibrium amounts or mole fractions of end members can only be found by GEM, if the bulk composition of C-S-H and the G^o_f value of each end member are known.

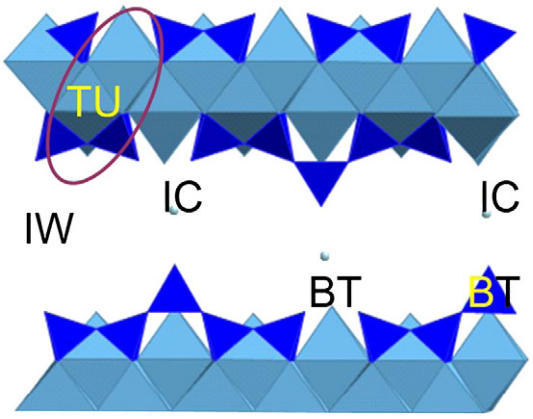

Fig. 2. Schematic representation of the defect tobermorite structure showing locations of the assumed sublattice sites and interlayer Ca^{2+} cations (H_2O molecules are not shown, all CU sites are vacant). See text for explanations.

In the Appendix A, the expansion of Eq. (7) into a list of 16 end-member formulae is shown in detail. Such a solid solution model appears to be far too complex and too difficult to parameterize, especially if substitutions in different sublattices are not independent. Therefore, a plausible route of reasonable simplification of the sublattice C-S-H solid solution model is discussed in the Appendix A. This route assumes (i) fixed IW site ratio of 4 at full H_2O occupancy, which limits the model to fully hydrated systems (100% RH); (ii) the inverse dependence of <CL> and Ca content in C-S-H, expressed through coupling substitutions in BT and CI sites into a combined BTI sublattice site, thus leading to a sublattice formula

$$\left[BTI^+\right]_2 : [TU^-]_2 : \left[CU^0\right]_2 : \left[IW^0\right]_4 \quad (8)$$

that results in four end members, connected via the reciprocal reaction:

$$JenH + T2C = TobH + J2C \quad (9)$$

with the molar Gibbs energy effect

$$\Delta G_{rcp} = G^o_{fTobH} + G^o_{fJ2C} - G^o_{fJenH} - G^o_{fT2C}. \quad (10)$$

The first assumption is $\Delta G_{rcp} = 0$. Because the JenH end member is assumed structurally to have infinite chain length CL, and the T2C end member is assumed to have CL = 2, their relative stability (manifested in ΔG_{rcp}) renders the solid solution model a certain dependence of mean <CL> on composition:

$$<CL> = \frac{3}{<v>} - 1 \quad \text{where } <v> = x_{T2C} + x_{J2C}. \quad (11)$$

Here, x denotes the end-member mole fraction, and $<v>$ is the average number of vacant silicate sites per dreierkette unit ($v_{T2C} = v_{J2C} = 1$ and $v_{TobH} = v_{JenH} = 0$, Table A.4). In terms of the ^{29}Si NMR-measured $<Q>$ ratio, $<Q> = Q1/(Q0 + Q1 + Q2\ldots)$, $<CL> \approx 2/<Q>$.

The CSHQ model has two independent substitutions in BTI and CU sublattices. Therefore, even in the case of ideal mixing (i.e. zero enthalpy and excess entropy of mixing [57,63]), the activity a_j of j-th

end member with i-th species in the BTI site and k-th species in the CU site is proportional to the product of site fractions $y^2_{j,BTI}\, y^2_{k,CU}$ defined as

$$y_{Si,BTI} = x_{TobH} + x_{JenH};\quad y_{Ca,BTI} = x_{T2C} + x_{J2C};$$
$$y_{Vcu,CU} = x_{TobH} + x_{T2C};\quad y_{CH,CU} = x_{JenH} + x_{J2C} \tag{12}$$

where the species are $Si_{0.5}OH^+$ (Si), $HO_{0.5}Ca^+_{0.5}$ (Ca), V_{CU} (Vcu), Ca $(OH)_2$ (CH), respectively, and x_j stand for the mole fractions of TobH, T2C, JenH and J2C end-members.

Sublattice SS models are not implicit in most geochemical codes (including PHREEQC and GEM-Selektor) where the ideal mixing is assumed to be simple, i.e. with the activity a_j of an end member equal to its mole fraction x_j, regardless of the number of end members [67,68]. Nevertheless, any ideal sublattice model can be implemented in such codes with help of a *fictive activity coefficient* $\lambda_j = a_j/x_j$. The end-member activity a_j is defined in a general way as

$$RT\ln a_j = \mu_j - G^o_{f,j} \tag{13}$$

μ_j is the chemical potential, defined in sublattice solid solutions ([57,63]) for e.g. TobH end member as

$$\mu_{TobH} = G^o_{fTobH} - y_{Ca,BTI}\, y_{CH,CU}\, \Delta G_{rcp} + RT(2\ln y_{Si,BTI} + 2\ln y_{Vcu,CU}) \tag{14}$$

assuming the zero excess term; ΔG_{rcp} is given by Eq. (10), and $G^o_f{}_j$ is the standard molar Gibbs energy of (pure) j-th end member. Eq. (14) is again different from the expression $\mu_j = (G^o_{fj} + RT\ln x_j)$ pertinent to the simple ideal mixing model. Hence, a fictive activity coefficient λ_j must be used for each end member. For instance,

$$\mu_{TobH} = (G^o_{fTobH} + RT\ln x_{TobH}) + RT\ln\lambda_{TobH},$$

where

$$\ln\lambda_{TobH} = 2\ln y_{Si,BTI} + 2\ln y_{Vcu,CU} - y_{Ca,BTI}\, y_{CH,CU}\frac{\Delta G_{rcp}}{RT} - \ln x_{TobH}. \tag{15a}$$

Similarly for other three end members,

$$\ln\lambda_{T2C} = 2\ln y_{Ca,BTI} + 2\ln y_{Vcu,CU} + y_{Si,BTI}\, y_{CH,CU}\frac{\Delta G_{rcp}}{RT} - \ln x_{T2C} \tag{15b}$$

$$\ln\lambda_{JenH} = 2\ln y_{Si,BTI} + 2\ln y_{CH,CU} + y_{Ca,BTI}\, y_{Vcu,CU}\frac{\Delta G_{rcp}}{RT} - \ln x_{JenH} \tag{15c}$$

$$\ln\lambda_{J2C} = 2\ln y_{Ca,BTI} + 2\ln y_{CH,CU} - y_{Si,BTI}\, y_{Vcu,CU}\frac{\Delta G_{rcp}}{RT} - \ln x_{J2C}. \tag{15d}$$

In the simplest case, ΔG_{rcp} (Eq. (10)) is assumed to be zero, and terms related to it disappear.

4. Modeling C-S-H Aq-SS chemical equilibria with GEM-Selektor code

Model calculations at room conditions ($T = 25$ °C $= 298.15$ K and $P = 1$ bar) were conducted using the GEM-Selektor v.2 and v.3 codes (http://gems.web.psi.ch) with the built-in Nagra-PSI chemical thermodynamic data base [70] (GEMS version), enhanced with the Cemdata'07 thermodynamic data set ([13], http://www.empa.ch/cemdata). Activity coefficients γ_j of aqueous species were calculated using the Davies equation in the form

$$\log_{10}\gamma_j = -A_\gamma Z_j^2\left(\frac{\sqrt{I}}{1+\sqrt{I}} - 0.3I\right) + \log_{10}x_W \tag{16}$$

where Z_j is the formula charge, x_W is the mole fraction of water-solvent (this term is used in GEM-Selektor code for correcting the Debye–Hückel-type activity coefficients from mole fraction to molality scale), $A_\gamma \approx 0.5114$ at $T = 25$ °C and $P = 1$ bar, and $I = \frac{1}{2}\sum_j m_j z_j^2$ is the effective ionic strength computed over molalities m_j of all charged aqueous species. The activity coefficient of water-solvent was set to unity according to the common practice for dilute aqueous systems. The model chemical system setup included aqueous electrolyte, gas mixture, portlandite (CH), amorphous silica (SH) phases, plus a variant of C-S-H SS phase. Relevant thermodynamic data are provided in Appendix B.

Calculations were conducted at 1 bar, 298.15 K in a 'forward modeling' fashion using the Process simulator of GEM-Selektor. The system recipes were constructed from 1000 g H_2O and 1 mol of SiO_2 plus variable addition of up to 2 mol $Ca(OH)_2$ (to change the composition of aqueous solution and C/S ratio in the solid part). 1 mol N_2 and 0.001 mol O_2 were added to set up the CO_2-free 'atmosphere'. The quality of model fit was estimated visually on the Process simulator plots. No formal least-square procedures were used because the main goal of this work was to find the most plausible one among simple (ideal) SS models with less degrees of freedom, rather than the most accurate non-ideal model with several empirical parameters fitted to a single experimental data set. Another reason for not using numerical regression was the difficulty in assigning weights and error intervals to the solubility data points collected from the literature.

Because there is no structural evidence for the existence of C-S-H solid solution at C/S<2/3, no solid solution between SH and tobermorite (such as CSH-I in the old SS model) has been considered. Instead, we assumed that the C-S-H solid solution phase co-exists with the SH (hydrous SiO_2) phase in the region 0.1<C/S<0.7. In this C/S interval, [Ca] and [Si] must be rather constant, and on the [Ca]–[Si] diagram, they both degenerate to a single point. Most of the solubility data available for the range 0.1<C/S<0.7 lie in the intervals 1 to 2 mM [Ca] and 3 to 5 mM [Si] and do not contradict this assumption. Using this data, the G^o_f value for TobH end member was adjusted first and then kept fixed. Provisional G^o_f value for the T2C (or T2) end member could be found by adjusting it to experimental data with C/S around 1.4–1.5 (or 1.2–1.3) in the solid part. Further adjustment involved the G^o_f value of J2C end members using data points with C/S between 1.25 until the appearance of CH phase. Next, the provisional G^o_f value of JenH end member was obtained from reaction (10) assuming $\Delta G_{rcp} = 0$. Further fitting to a particular data set has been done, if necessary, by slightly re-adjusting G^o_f values of some end members. The resulting parameter values are provided in part in Appendix A and in the main text below.

4.1. The initial CSHQ model

All variants of the reciprocal CSHQ model based on Eqs. (9)–(15) yield the "best" visual fit (see Appendix A for details) similar to that of the C-S-H ideal SS model from Cemdata'07 database (see Fig. 1), i.e. relatively good for $[Ca]_{AQ}$ with the over-prediction of $[Si]_{AQ}$ at C/S>1.0. The [Si] and [Ca] curves cross at C/S<0.7, whereas the majority of experimental data suggest the cross-over at 0.8<C/S<0.9. Because the region at 0.8<C/S<1.1 is important especially in degraded OPC and low-Ca cements, a more elaborate and structurally realistic C-S-H solid solution model is necessary. There are indications that at C/S≈1, a relatively ordered pentameric C-S-H compound exists in tobermorite-like nanocrystalline C-S-H [22]. If this intermediate compound is relatively stable, it should strongly affect the shapes of C-S-H solubility curves.

4.2. Development of the CSH3T model

To explore this idea, the sublattice CSHQ model elaborated in Appendix A was modified by assuming that all CU sites are vacant (i.e. removing JenH and J2C end members), and by adding a 'fictive' T5C end member with C/S = 1. This new model is now a ternary ideal solid

solution of three end members TobH, T5C and T2C, related entirely to the defect-tobermorite structure, hence it will be called a 'CSH3T' model. The 'pentameric' end member T5C is introduced to represent an intermediate ordered compound. This CSH3T model of the type $(A,B)_2X$ is assumed to behave similar to the calcite $Ca_2(CO_3)_2$–dolomite $CaMg(CO_3)_2$–magnesite $Mg_2(CO_3)_2$ system described by Holland and Powell ([71], p. 497–498). In their formalism, the ordering is represented using two sublattices (A,B)(A,B)X, which is followed here (except the excess energy terms) using $Si_{0.5}OH^+$ and $HO_{0.5}Ca^+_{0.5}$ BTI species in places of A (Ca) and B (Mg), respectively. Conversely, the sublattice formula of C-S-H becomes

$$\left[BTI1^+\right]_1: \left[BTI2^+\right]_1: [TU^-]_2: \left[CU^0\right]_2: \left[IW^0\right]_4 \quad (17)$$

which leads to three end members defined in Table 2. Being derived from structural features of tobermorite-like C-S-H, the CSH3T model is restricted in composition to phases with C/S<1.5.

The Gibbs energy effect ΔG_{ord} for the internal equilibrium reaction 0.5TobH + 0.5T2C = T5C

$$\Delta G_{ord} = G^o_{f\ T5C} - 0.5G^o_{f\ TobH} - 0.5G^o_{f\ T2C} \quad (18)$$

defines the extent of ordering and the relative stability of the T5C end member. The activities of end members for the ideal mixing of $Si_{0.5}OH^+$ and $HO_{0.5}Ca^+_{0.5}$ species on BTI1 and BTI2 sites are expressed through site fractions $y_{BTI1,Si}$; $y_{BTI1,Ca}$; …, and end member mole fractions x_j as

$$\begin{aligned} a_{TobH} &= y_{Si,BTI2}\, y_{Si,BTI1} = (x_{TobH} + x_{T5C})x_{TobH} \\ a_{T5C} &= y_{Si,BTI2}\, y_{Ca,BTI1} = (x_{TobH} + x_{T5C})(x_{T2C} + x_{T5C}) \\ a_{T2C} &= y_{Ca,BTI2}\, y_{Ca,BTI1} = x_{T2C}(x_{T2C} + x_{T5C}) \end{aligned} \quad (19)\text{a, b, c}$$

leading to fictive activity coefficients used in GEM-Selektor calculations:

$$\begin{aligned} \ln\lambda_{TobH} &= \ln(x_{TobH} + x_{T5C}) \\ \ln\lambda_{T5C} &= \ln(x_{TobH} + x_{T5C}) + \ln(x_{T2C} + x_{T5C}) - \ln x_{T5C} \\ \ln\lambda_{T2C} &= \ln(x_{T2C} + x_{T5C}). \end{aligned} \quad (20)$$

The mean silicate chain length is now recovered as

$$<CL> = \frac{3}{<v>} - 1 \quad \text{where } <v> = x_{T2C} + 0.5x_{T5C}. \quad (21)$$

By adjusting G^o_f values of end members, the CSH3T ideal model can easily be set (Table 3) to reproduce the generic C-S-H solubility data in a quite reasonable way. As seen on Fig. 3, this model behaves surprisingly well. Unlike the CSHQ model (Appendix A), it reproduces correctly the congruence point (near crossing of $[Ca]_{AQ}$ and $[Si]_{AQ}$ curves) in C/S-[Ca], C/S-[Si], and [Ca]–[Si] spaces. Fig. 3 shows that the relative stability of T5C compound, and, hence, the extent of ordering, is rather high. The activity of TobH end member a_{TobH} closely follows the site fraction $y_{Si,BTI1} = x_{TobH}$; likewise, a_{T2C} follows $y_{Ca,BTI2} = x_{T2C}$, and everywhere, except a very narrow interval near C/S = 1, a_{T5C} follows $x_{T5C} = 1 - x_{T2C} - x_{TobH}$. Thus, it is not surprising that setting

Table 2
CSH3T SS model with ordering in two BTI sublattices in pentameric T5C end member.

End member				Structural sublattice formula	CL	Bulk formula
ID	u	v	y			
TobH	2	0	0	$[Si_{0.5}OH^+]_1$:$[Si_{0.5}OH^+]_1$:$[CaSiO^-_{3.5}]_2$: $[V_{CH}]_2$: $[H_2O]_4$	∞	$[(CaO)_{2/3}SiO_2 (H_2O)_{5/3}]_3$
T5C	1	0.5	1	$[Si_{0.5}OH^+]_1$:$[HO_{0.5}Ca^+_{0.5}]_1$:$[CaSiO^-_{3.5}]_2$: $[V_{CH}]_2$:$[H_2O]_4$	5	$[(CaO)_1SiO_2 (H_2O)_2]_{2.5}$
T2C	0	1	2	$[HO_{0.5}Ca^+_{0.5}]_1$:$[HO_{0.5}Ca^+_{0.5}]_1$: $[CaSiO^-_{3.5}]_2$: $[V_{CH}]_2$:$[H_2O]_4$	2	$[(CaO)_{3/2}SiO_2 (H_2O)_{5/2}]_2$

CL is the theoretical silicate chain length.

Table 3
CSH3T ideal SS model parameters, adjusted against the generic C-S-H solubility data.

End member	Bulk formula	G^o_f, in kJ mol^{-1}	$\log_{10}K$
TobH	$(CaO)_2(SiO_2)_3(H_2O)_5$	−5121.92	−12.20
T5C	$(CaO)_{2.5}(SiO_2)_{2.5}(H_2O)_5$	−5036.18	−13.74
T2C	$(CaO)_3(SiO_2)_2(H_2O)_5$	−4931.88	−12.03

Normalized per 3 tetrahedral sites; ordering model with two BTI sites; $\Delta G_{ord} = -9.28$ kJ/mol; K is the equilibrium constant of the reaction $(CaO)_x(SiO_2)_y(H_2O)_z = ySiO_2 + xCa(OH)_2 + (z-x)H_2O$ (data for amorphous silica SiO_2, portlandite $Ca(OH)_2$ and water H_2O are given in Appendix B).

$\ln\lambda_{TobH} = 0$, $\ln\lambda_{T5C} = 0$ and $\ln\lambda_{T2C} = 0$ results in calculated solubility diagrams that are almost identical to Fig. 3 A,B. In other words, the CSH3T ideal sublattice model (Eqs. (19) and (20); Tables 2 and 3) behaves like a ternary SS model with simple ideal mixing. This might explain the partial success of old simple ideal binary C-S-H SS models with tobermorite-like end members having C/S of 0.83 (see Table 1), i.e. close to C/S = 1.

In trial GEM calculations, the impact of ΔG_{ord} parameter has been checked by running the CSH3T model with G^o_{fT5C} value set 8.0 kJ mol^{-1} more positive. This change did not affect the calculated <CL> curve as function of C/S ratio; <CL> was also found independent of large variations in stability of TobH and T2C end members. However, activities of end members significantly deviated from site- and mole fractions (see thin dash-dot curves on Fig. 3 B,D); the fit to solubility data became much worse, resembling that of the CSHQ reciprocal model. Hence, the match of CSH3T model to the solubility data depends mainly on the ΔG_{ord} parameter which must have a negative value about −9 kJ mol^{-1}.

The CSH3T solid solution model (Table 3) is a 'basis' model for further modifications. To extend it with other cations (Sr, Na, K, U(VI), …) expected to enter only the BTI positions, one would need to introduce the analogs of T2C and/or T5C end members and account for their site fractions in activity and configurational entropy terms. Thus extended solid solution model should be sufficient for modeling the solubility and stability of C-S-H in cement pore waters with pH>13. In this context, the CSH3T model provides a good starting point for modeling sorption of various cations in C-S-H.

Within the CaO–SiO_2–H_2O system, the CSH3T model can be further improved in two ways.

(1) The excess mixing parameters can be introduced and fitted to the phase equilibrium data (as done in the calcite–magnesite–dolomite SS model [71]).
(2) The ideal sublattice model can be modified for different stoichometry ratios of sublattice sites. The latter choice appears to be more appropriate for keeping the SS model of C-S-H as simple as possible.

By trying approach (2), an even better fit to solubility data has been obtained when the end-member activities and fictive activity coefficients were represented as

$$\begin{aligned} a_{TobH} &= y^2_{Si,BTI2} y^2_{Si,BTI1} \\ a_{T2C} &= y^2_{Ca,BTI2} y^2_{Ca,BTI1} \\ a_{T5C} &= y^2_{Si,BTI2} y^2_{Ca,BTI1} \end{aligned} \quad (22)$$

$$\begin{aligned} \ln\lambda_{TobH} &= \ln x_{TobH} + 2\ln(x_{TobH} + x_{T5C}) \\ \ln\lambda_{T5C} &= 2\ln(x_{TobH} + x_{T5C}) + 2\ln(x_{T2C} + x_{T5C}) - \ln x_{T5C} \\ \ln\lambda_{T2C} &= 2\ln(x_{T2C} + x_{T5C}) + \ln x_{T2C}. \end{aligned} \quad (23)$$

This is equivalent to doubling the number of BTI1 and BTI2 sites per unit formula of TobH, T5C and T2C end members according to a modified sublattice scheme

$$\left[BTI1^{+0.5}\right]_2: \left[BTI2^{+0.5}\right]_2: [TU^-]_2: \left[CU^0\right]_2: \left[IW^0\right]_4, \quad (24)$$

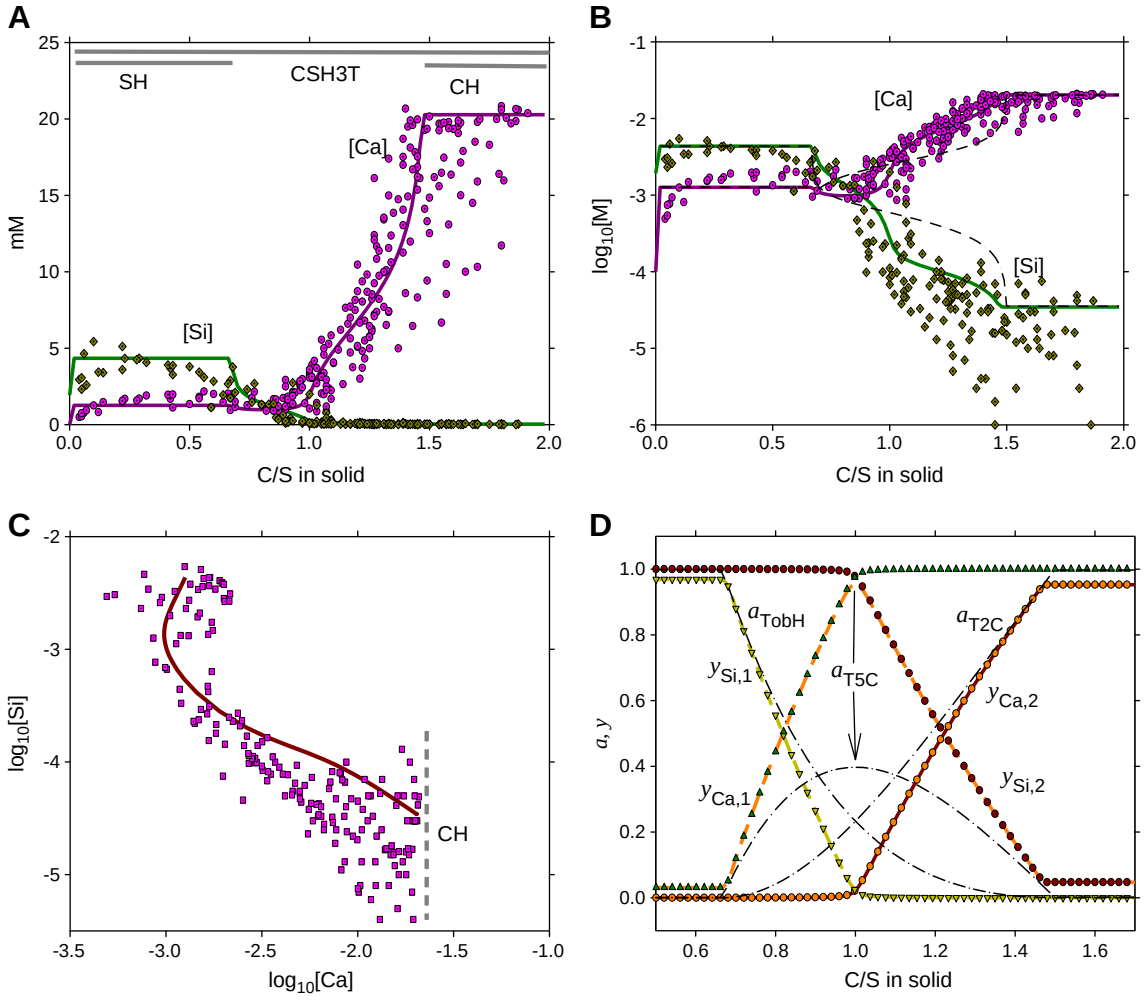

Fig. 3. The generic CSH3T model from Table 3 (curves). Scattered symbols on (A), (B), (C) represent the literature data collected from Refs. [18,39–41,43–45]. On (D) diagram, the site fractions $y_{Si,BTI1}$ or $y_{Si,BTI2}$ correspond to $[Si_{0.5}OH^{+}]$, and $y_{Ca,BTI1}$ or $y_{Ca,BTI2}$ to $[HO_{0.5}Ca_{0.5}^{+}]$ species. Site fractions were computed from Eqs. (20), (21), and end member activities (a_{TobH}, a_{T5C}, a_{T2C}) from Eq. (19). Thin dash-dot curves on (B) and (D) show the model variant with 8 kJ mol^{-1} more positive ΔG_{ord} (see text for explanations).

where species $Si_{0.25}O_{0.5}H_{0.5}^{+0.5}$ and $H_{0.5}O_{0.25}Ca_{0.25}^{+0.5}$ substitute each other in BTI1 or BTI2 sublatice sites. The bulk end-member stoichiometry and mean chain length are unaffected.

To check how this CSH3T model reproduces <CL>, the set of 'double decomposition' (curve C″) C-S-H samples data [18] has been selected because this set includes the solubility data for de/recalcification cases together with the ^{29}Si NMR <CL> data measured on some samples. Chen et al. [18] also concluded that curve C″ samples have minimal Ca–OH content and a close resemblance to 1.4-nm tobermorite. Besides, to our knowledge, the <CL> data for C-S-H samples going along the curve A assuming purely tobermorite-like structure are not available. Indeed, after some adjustment of G_f^o values of end members (while the ΔG_{ord} value remained close to −9 kJ mol^{-1}), the CSH3T model (Table 4, Fig. 4) reproduced quite well both the <CL> and the solubility (curve C″) data. The quality of fit in all four diagrams was found to be so good that further complication of the SS model by introducing excess Gibbs energy terms was not warranted.

Disabling the fictive activity coefficients (i.e. running the model with $a_j = x_j$) results in the shapes of solubility curves similar to those obtained using the earlier model with 2 BTI sites (either sub-lattice or simple ideal mixing variant), see Fig. 3. From Eqs. (22), (23) it follows that scaling the end member stoichiometry in CSH3T SS model down by a factor of 2 will result in a new sublattice scheme

$$\left[BTI1^{+0.5}\right]_1 : \left[BTI2^{+0.5}\right]_1 : \left[TU^{-}\right]_1 : \left[CU^{0}\right]_1 : \left[IW^{0}\right]_2, \tag{25}$$

with the ideal mixing on sublattices described by equations for activities and fictive activity coefficients identical to Eqs. (19) and (20). This "downscaled" CSH3T model (Table 5), either with Eqs. (19)–(21) or using the simple ideal mixing (by forcing $\ln\lambda_{TobH} = 0$, $\ln\lambda_{T5C} = 0$ and $\ln\lambda_{T2C} = 0$) produces the same curves as shown on Fig. 4, which also look pretty consistent to the whole collection of literature solubility data (Fig. 5).

Note that end member stoichiometries in Table 5 resemble those in the old binary CSH SS model [10,13] where the optimized end member formulae had n_{Si} factors between 1 and 2 (see Table 1). However, the new CSH3T model differs in that it is a single ternary solid solution covering the C/S range between 0.67 and 1.5; it co-exists with SH (at C/S<0.7) or with CH (at C/S>1.45) pure phases; and it has a correct built-in dependence of <CL> on C/S ratio.

Table 4
The CSH3T ideal sublattice model with four BTI sites.

EM	Bulk formula	G_f^o, kJ mol^{-1}	$\log_{10}K$
TobH	$(CaO)_2(SiO_2)_3(H_2O)_5$	−5123.06	−12.40
T5C	$(CaO)_{2.5}(SiO_2)_{2.5}(H_2O)_5$	−5037.32	−13.94
T2C	$(CaO)_3(SiO_2)_2(H_2O)_5$	−4934.16	−12.43

Formulae are normalized per 3 tetrahedral sites; $\Delta G_{ord} = -8.71$ kJ/mol; see also notes to Table 3.

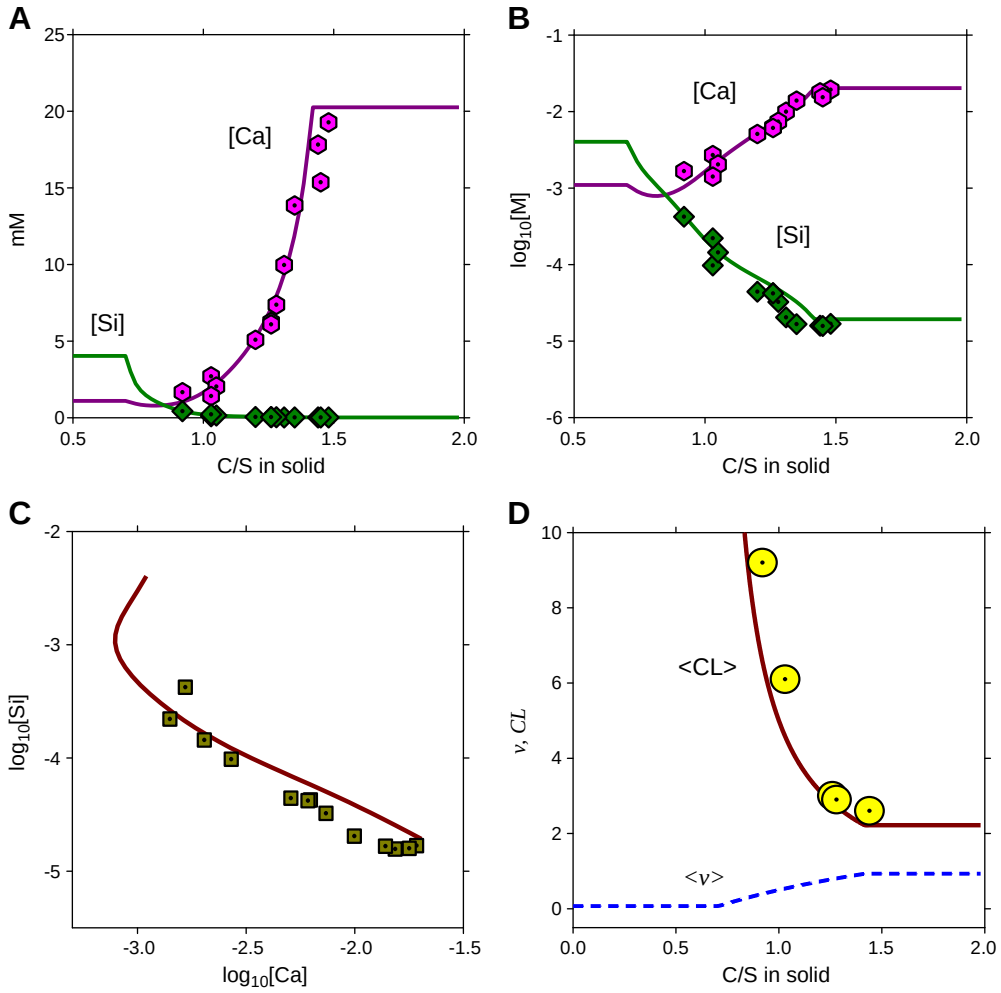

Fig. 4. The CSH3T SS model with 4 BTI sites (Table 4, Eqs. (22)–(24)) adjusted to the data [18] for C-S-H 'double decomposition' samples (Curve C″), shown as large scattered symbols. On (D), <*v*> is the fraction of silica dimers; <CL> is the mean silica chain length (Eq. (21)), plotted against <CL> estimates from ^{29}Si NMR data (dotted circles) from (Table 4 in Ref. [18]).

Unfortunately, the CSH3T model cannot account for C-S-H phases that are relatively more polymerized and go above C/S = 1.5, as, for example, the C solubility curve for the C3S hydration data on Chen et al. [18] solubility diagram, presumably corresponding to higher Ca–OH content, longer mean chain length, and significant role of the 'jennite-like' component. However, the structure of such phases remains ambiguous; it not quite clear, whether jennite or interstitial CH structural domains exist there. Hence, at present, it would not make sense to extend the CSH3T model above C/S = 1.5 because this cannot be justified on the basis of the available structural information.

4.3. The downscaled CSHQ SS model

Let us recall the ability of simple ideal solid solution models of C-S-H to yield a better fit to the solubility data with the downscaled end member stoichiometry [10], as also shown here for the CSH3T model (Table 5, Fig. 5). Such reduction to simple ideal mixing is rigorous, if there is a substitution in one sublattice only. As explained in ([58] p. 41–42), the ideal sublattice solid solution $(A,B)_2X$ with end members A_2X and B_2X has the site fractions of A and B equal to mole fractions x_{A2X} and x_{B2X}, respectively, and end member activities $a_{A2X} = x^2_{A2X}$ and $a_{B2X} = x^2_{B2X}$. These can be accommodated to the simple ideal mixing model (where $a_j = x_j$) either by introducing the fictive activity coefficients ($\lambda_{A2X} = x_{A2X}$; $\lambda_{B2X} = x_{B2X}$), or by dividing the stoichiometry of both end members (and their G_f^o values) by 2, which leads to $a_{AX0.5} = x_{AX0.5}$ and $a_{BX0.5} = x_{BX0.5}$. Such downscaling of end members is not always rigorous because, if there are two or more sublattices with independent substitutions, some configurational entropy terms will be neglected by the simple ideal mixing model.

Yet, the downscaling may improve the description of solubility/stability data in a semi-empirical way [10] when the substitution mechanisms or the sublattice ratios are not clear. Compared with classic excess energy models (e.g. regular), the empirical 'fit' will be embedded not in interaction parameters, but directly into formula scaling factors and in G_f^o values of end members. This may be a good workaround to keep things simple for the defect tobermorite–jennite based solid solution models of C-S-H, until more rigorous and atomistically reasonable multi-site (sublattice) solid solution models will become available.

Back to the CSHQ model (Appendix A, Table A.6), we attempted re-scaling its end members from three to one tetrahedral site (dividing by factor of 3), as shown in Table 6, and use them within simple ideal mixing model (having all end-member activity coefficients set to 1.0).

Table 5
The downscaled simple ideal CSH3T SS model.

End member	Bulk formula	G_f^o, kJ mol^{-1}	$\log_{10}K$
TobH	$(CaO)_{1.0}(SiO_2)_{1.5}(H_2O)_{2.5}$	−2561.53	−6.20
T5C	$(CaO)_{1.25}(SiO_2)_{1.25}(H_2O)_{2.5}$	−2518.66	−6.97
T2C	$(CaO)_{1.5}(SiO_2)_{1.0}(H_2O)_{2.5}$	−2466.99	−6.22

Normalized per 1.5 tetrahedral sites; $\Delta G_{ord} = -4.40$ kJ/mol; see also notes to Table 3.

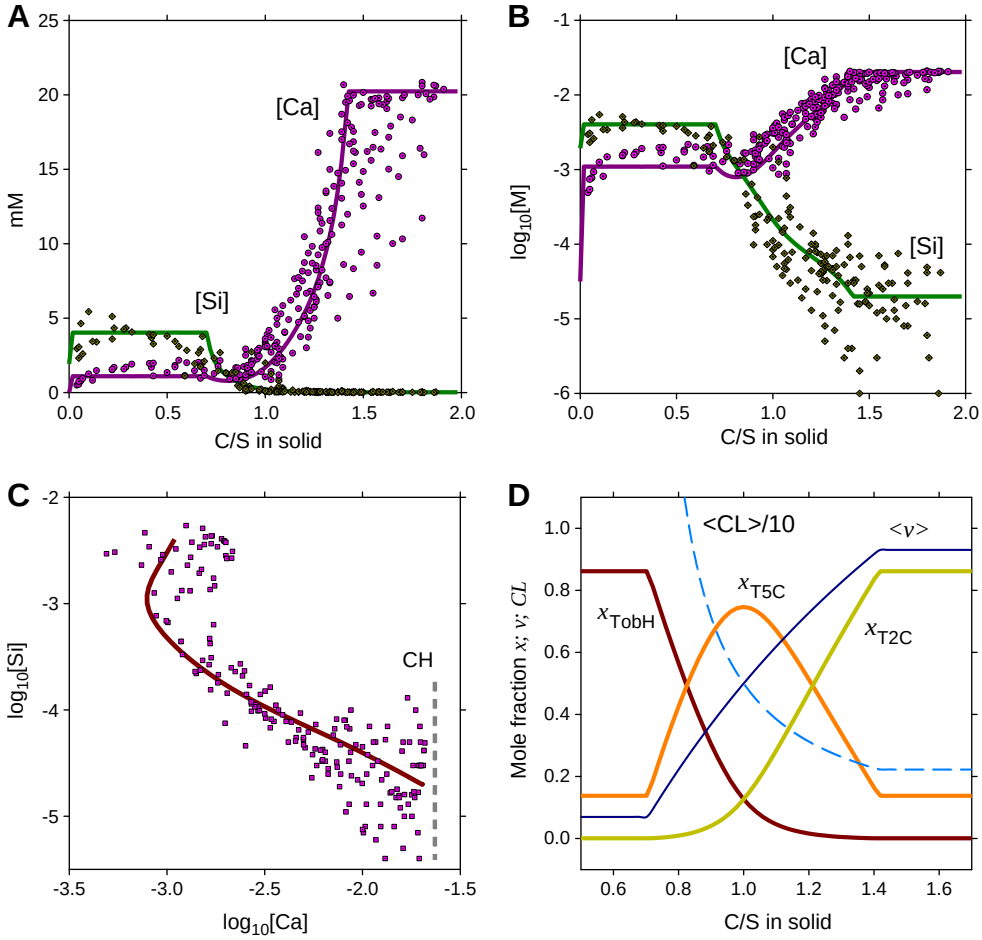

Fig. 5. The downscaled CSH3T ideal solid solution model (Table 5, curves) vs the literature C-S-H solubility data [18,39–41,43–45] (scattered points), shown as function of C/S in the solid in linear scale (A), $\log_{10}$ scale (B), on a logarithmic [Ca]–[Si] diagram (C), and as CSH3T phase composition (D). The fraction of silica dimers <*v*> and the mean chain length <CL> were calculated using Eq. (21).

In forward GEM modeling, it was possible to obtain a reasonable description of the generic C-S-H solubility data in the whole C/S interval with $G^{o}_{f\,\mathrm{TobH}} = -1668.56$; $G^{o}_{f\,\mathrm{TobD}} = -1573.46$; $G^{o}_{f\,\mathrm{JenD}} = -2170.32$, and $G^{o}_{f\,\mathrm{JenH}} = -2265.42$ kJ/mol ($\Delta G_{\mathrm{rcp}} = 0$). However, only three end members appear significant there, while the x_{JenH} never exceeds 1%, and the mean chain length obtained as

$$<CL> = \frac{3}{x_{TobD} + x_{JenD}} - 1 \qquad (26)$$

is underestimated with respect to both 'C_3S hydration' and 'double decomposition' data from [18]. Obviously, a more stable JenH end member is needed to improve the SS model, especially against the C_3S hydration data, presumably reflecting a significant amount of Ca-OH manifesting the extensive presence of jennite-like C-S-H structure (along the curve C on the solubility diagram [18]). For the C_3S hydration series, the solubility data were provided together with the ^{29}Si MAS NMR data, from where the <CL> data was determined [18].

We were able to fit these <CL> data well with the downscaled CSHQ simple ideal model, which simultaneously yields a good fit to solubility data ([18], Curve C) in [Ca]–[Si] and C/S–[Ca], C/S–[Si] spaces. Results are shown on Fig. 6 and in Table 6.

The reciprocal molar Gibbs energy effect ΔG_{rcp} (Eq. (10)) appears to control the values of <CL> estimated from the mole fractions of dimeric end members (Eq. (11)). The model underestimates $[\mathrm{Si}]_{\mathrm{AQ}}$ at C/S 0.8–0.9 because it neglects the ordering effects near C/S = 1. Yet, the performance of this really simple ideal model is remarkable and sufficient for most practical applications in cement chemistry. Thus, the semi-rigorous downscaled CSHQ model appears to be free from most drawbacks of the old CSH-I–CSH-II model [10].

It seems not to be warranted improving the model fits either by re-scaling end members with separate scaling factors, or by introducing excess Gibbs energy parameters. One should keep in mind that in reality, many metastable C-S-H phases are possible, each with a unique dependence of chain length and –Ca–OH content on composition [18], depending on the preparation route and temperature, as well as on the equilibration conditions and aging time. So, after each adjustment of G^{o}_{f} values of end members, the downscaled CSHQ model becomes, in fact, a solid solution model of a different metastable C-S-H phase.

Table 6
The improved downscaled CSHQ simple ideal solid solution model (Fig. 6).

End member	C/S	CL	Bulk formula	G^{o}_{f}, in kJ mol^{-1}	$\log_{10}K$	$\pm \log_{10}K$
TobH	2/3	∞	$(CaO)_{2/3}(SiO_2)_{1.0}(H_2O)_{3/2}$	−1668.56	−4.20	−0.4 + 0.2
TobD (T2)	5/4	2	$(CaO)_{5/6}(SiO_2)_{2/3}(H_2O)_{11/6}$	−1570.89	−3.55	−0.6 + 0.2
JenH	4/3	∞	$(CaO)_{4/3}(SiO_2)_{1.0}(H_2O)_{13/6}$	−2273.99	−5.51	−0.3 + 0.5
JenD (J2)	9/4	2	$(CaO)_{3/2}(SiO_2)_{2/3}(H_2O)_{5/2}$	−2169.56	−3.66	−0.3 + 0.4

Reciprocal reaction: JenH + TobD = TobH + JenD with $\Delta G_{\mathrm{rcp}} = +6.76$ kJ mol^{-1}. $\log_{10}K$ for reaction (28).

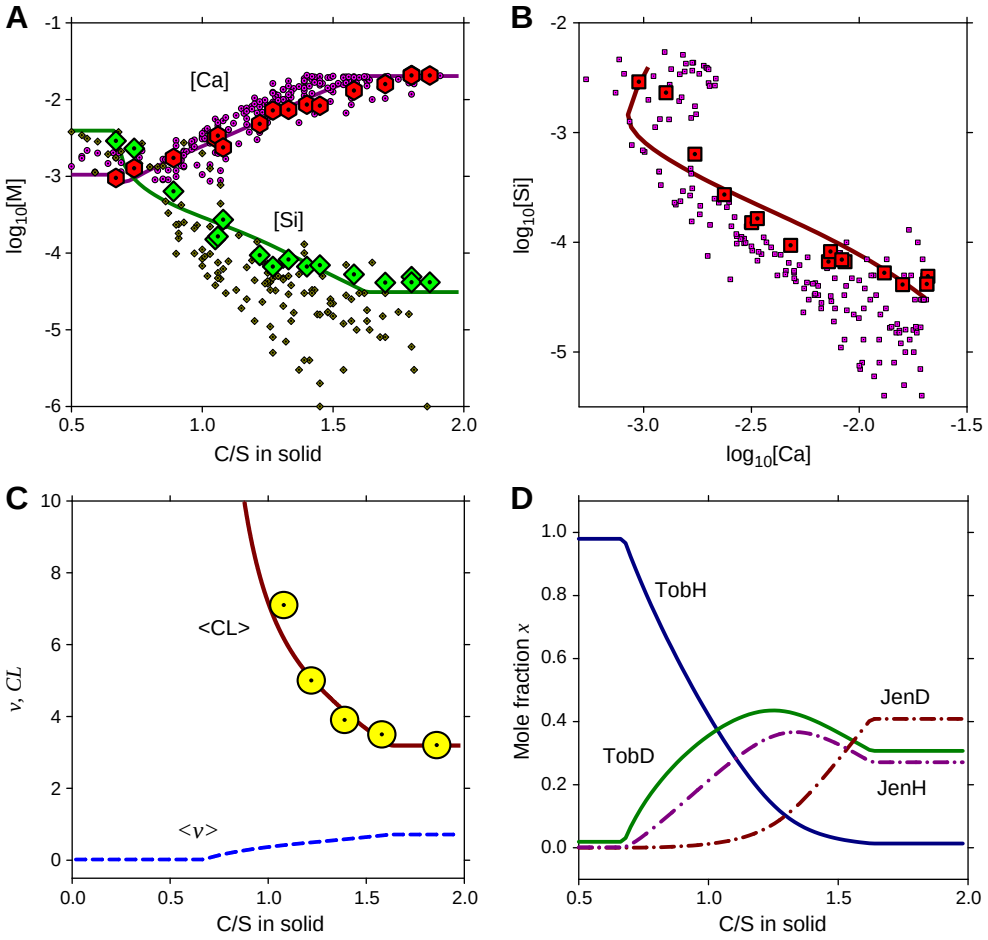

Fig. 6. The downscaled CSHQ model (Table 6) adjusted to the C3S hydration (C-curve) data from [18], large scattered symbols, on the background of other literature data (small scattered symbols). On (C), <*v*> is the fraction of silica dimers; <CL> is the mean silica chain length (Eq. (26)), plotted against <CL> estimates from ^{29}Si NMR data (large dotted circles) from (Table 4 in Ref. [18]). Graph (D) shows predicted mole fractions of CSHQ end members.

As shown in detail in a model sensitivity study (see Appendix C, Supplementary Information file), by moderate re-adjustments of end member G_f^o values within 0.2 to 0.6 pK units (1.2 to 3.3 kJ mol^{-1}), the simple ideal CSHQ model can provide at best a good, at least a reasonable description of each of several available literature data sets [18,39–41,43–45]. The respective uncertainty brackets for the end member solubility products are included in Table 6. This sensitivity study showed also that in some old data sets, the [Si] data below 10^{-5} M may be out of equilibrium with C-S-H or in large (systematic?) analytical error.

4.4. Density, molar volume, entropy and heat capacity of CSH3T and CSHQ end members

Realistic prediction of density of C-S-H 'gels' (at least in H_2O saturated state) is especially important in reactive transport modeling, where volume changes due to dissolution or precipitation of solid phases may affect the porosity and the transport parameters.

As stated in Section 2.2, the 'variable gel water' (VGW) case [9] appears to be more appropriate than the 'constant gel water' (CGW) case, except for the nanocrystalline C-S-H [22]. Thus, we can assume that the density of C-S-H solid solutions is limited between VGW and CGW cases. As seen on Fig. 7, this is possible, if densities of pure TobD and T2C end members match the VGW case, while the ordered T5C (pentameric) compound is somewhat denser than the T2C (dimeric) end member of CSH3T solid solution. It is expected that the density of C-S-H SS phases in H_2O-saturated state lies within the triangle "TobH–TobD–crossing of CGW and VGW curves", and this should be reproduced by both CSH3T and CSHQ solid solution models.

Standard molar volumes of end members listed in Table 7 were calculated from end member formulae and from densities shown on

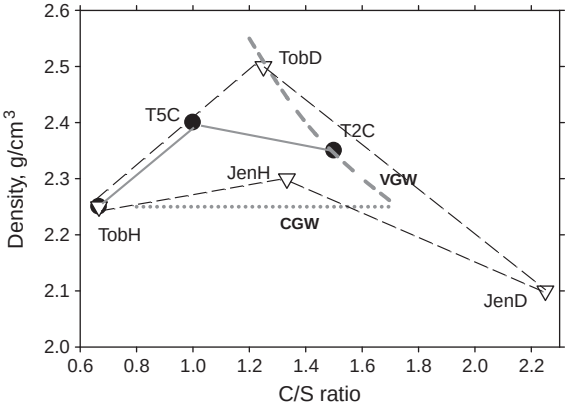

Fig. 7. Assumed densities of CSH3T (solid circles) and CSHQ (open triangles) SS end members. CGW (dotted) is the 'constant gel water', and VGW (dashed) is the 'variable gel water' trend curve corresponding to (Fig. 6 in Ref. [9]). Thin solid lines show possible CSH3T phase densities; thin dashed lines mark the area of possible CSHQ solid solution densities.

Table 7
Density and molar volume of CSHQ and CSH3T SS end members ($\Delta_r V^o$ for Eq. (28)).

End member	Bulk formula	G^o_f, in kJ mol^{-1}	ρ_{sat}, g cm^{-3}	V^o, cm^3 mol^{-1}	$\Delta_r V^o$ cm^3 mol^{-1}
TobH	$(CaO)_{2/3}SiO_2(H_2O)_{3/2}$	−1668.56	2.25	55.30	10.8
TobD	$(CaO)_{5/6}(SiO_2)_{2/3}(H_2O)_{11/6}$	−1570.89	2.50	47.95	17.0
JenH	$(CaO)_{4/3}SiO_2(H_2O)_{13/6}$	−2273.99	2.30	75.63	12.5
JenD	$(CaO)_{3/2}(SiO_2)_{2/3}(H_2O)_{5/2}$	−2169.56	2.10	80.58	6.41
TobH	$(CaO)_1(SiO_2)_{3/2}(H_2O)_{5/2}$	−2561.53	2.25	84.96	18.7
T5C	$(CaO)_{5/4}(SiO_2)_{5/4}(H_2O)_{5/2}$	−2518.66	2.40	79.27	20.9
T2C	$(CaO)_{3/2}(SiO_2)_1(H_2O)_{5/2}$	−2467.08	2.35	80.56	16.1

Fig. 7. These volumes (here assumed to be independent of temperature and pressure) also define the corrections of molar Gibbs energy function $g_{T,P}$ of a C-S-H end member up to a few hundred bar pressure P:

$$g_{T,P} = g^o_T + V^o(P-1). \quad (27)$$

The dependence of g^o_T function ($g^o = G^o_f$ at $T_r = 298.15$ K) on the elevated temperature T (up to 370 K) requires knowledge of standard molar entropy S^o and heat capacity Cp^o of C-S-H SS end members at T_r. For the old CSH-II ideal SS model end members, these parameters were evaluated by Lothenbach et al. [13] and included in Cemdata'07 data base (see also http://gems.web.psi.ch/doc/pdf/ for the overview of T,P correction methods).

In the present study, thermodynamic properties of C-S-H solid solution end members were calculated using standard-state effects of the reaction

$$\underset{\text{C-S-H end member}}{(CaO)_xSiO_2)_y(H_2O)_z} = \underset{\text{am.silica}}{ySiO_2} + \underset{\text{portlandite}}{xCa(OH)_2} + \underset{\text{water}}{(z-x)H_2O} \quad (28)$$

From the data [13] (see also Table 1), we find for the reaction (28) for Tob-II (C/S = x/y = 0.83) and Jen-II (C/S = 1.67) end members, respectively, $\Delta_r S^o = 65.5$ and 70 J K^{-1} mol^{-1}; and $\Delta_r Cp^o = 22$ and 12 J K^{-1} mol^{-1}. Both parameters weakly depend on C-S-H composition; the differences are less than 10 J K^{-1} mol^{-1}, so the linear dependencies of both reaction effects on x = C/S ratio (for y = 1 and C/S = x/y) can be assumed:

$$\Delta_r S^o = 61.054 + 5.357x \quad (29a)$$

$$\Delta_r Cp^o = 31.881 - 11.905x. \quad (29b)$$

Using Eqs. (29a), (29b) and (28), $\Delta_r S^o$ and $\Delta_r Cp^o$ were calculated for y = 1 and x = C/S, then re-scaled to values of y used in the formulae of downscaled CSHQ and CSH3T end members, and rounded off to zero digits after decimal point. The resulting values (Table 8) are expected to be sufficient for temperature corrections from 0 to 90 °C within 0.5 pK units uncertainty. The $\Delta_r H^o$ values were calculated from log$K$ and $\Delta_r S^o$ values together with the S^o, Cp^o and H^o values all at $T_r = 298.15$ K using the ReacDC module of GEM-Selektor code.

Table 8
Effects of reaction (28) at $P = 1$ bar, $T_r = 298.15$ K, with standard molar S^o, Cp^o and H^o values of the downscaled CSHQ and CSH3T SS model end members.

End member	$\log_{10}K$	$\Delta_r H^o$ kJ mol^{-1}	H^o kJ mol^{-1}	$\Delta_r S^o$ J K^{-1} mol^{-1}	S^o J K^{-1} mol^{-1}	$\Delta_r Cp^o$ J K^{-1} mol^{-1}	Cp^o J K^{-1} mol^{-1}
TobH	−4.20	43.35	−1841.51	65	89.9	24	141.6
TobD	−3.55	33.68	−1742.42	45	121.8	11	166.9
JenH	−5.51	51.73	−2506.27	68	142.5	16	207.9
JenD	−3.66	35.50	−2400.72	49	173.4	3.4	232.8
TobH	−6.20	64.31	−2832.98	97	152.8	36	231.2
T5C	−6.97	64.53	−2518.66	83	159.9	25	234.1
T2C	−6.22	55.96	−2722.30	69	167.0	14	237.0

4.5. Density, volume and H_2O content as function of C/S ratio

Using the data from Tables 7 and 8, as well as from Appendix A (Table A.6), not only the solubilities, but also the variations of density, molar volume, interlayer (non-hydroxyl) H_2O mole fraction, and H/S ratio (i.e. total bulk H_2O content per 1 mol SiO_2) (Fig. 8) in the CSH3T or CSHQ phase were calculated in GEM-Selektor at ambient conditions, as follows (x_j is mole fraction of j-th end member):

$$\rho_{CSH} = \sum_j \rho_j x_j; \quad V_{CSH} = \sum_j V^o_j x_j. \quad (30a, b)$$

For the CSH3T SS model (Tables 2 and 5), the water contents were calculated as:

$$y_{H2O,IL} = 2(x_{TobH} + x_{T5C} + x_{T2C}) \quad (31a)$$

$$(H/S)_{(H2O,bulk)} = 5/3x_{TobH} + 2x_{T5C} + 5/2x_{T2C} \quad (31b)$$

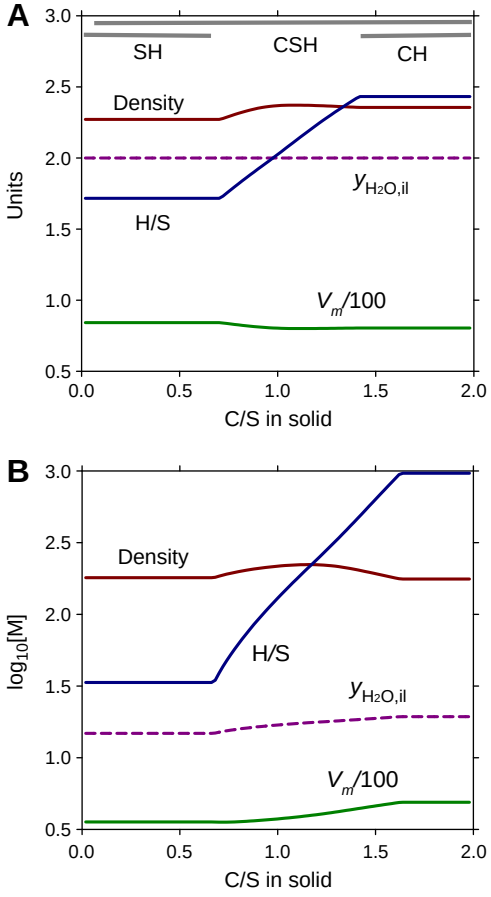

Fig. 8. Variations of density (in g cm^{-3}), volume V_m (in cm^3 mol^{-1}), interlayer H_2O mole fraction $y_{H2O,il}$, and H_2O/SiO_2 mole ratio H/S of the C-S-H phase, as predicted by the downscaled CSH3T simple ideal model Table 5 (A) and by the downscaled CSHQ simple ideal model Table 6 (B).

For the CSHQ SS model (using Tables A.6 and 6):

$$y_{H2O,IL} = 7/6\left(x_{TobH} + x_{JenH}\right) + 8/6\left(x_{TobD} + x_{JenD}\right) \quad (32a)$$

$$(H/S)_{(H2O,bulk)} = 9/6\, x_{TobH} + 13/6\, x_{JenH} + 11/4\, x_{TobD} + 15/4\, x_{JenD}. \quad (32b)$$

Results obtained from Eq. (31b) have been regressed ($r^2 = 0.999$) with a function H/S = 1 + C/S yielding the CSH3T SS bulk composition model ($(CaO)_xSiO_2(H_2O)_{1+x}$) valid up to C/S = 1.5. Regression of results from Eq. (32b) yields H/S = 0.614 + 1.392(C/S), leading to a bulk stoichiometry formula of CSHQ phase $(CaO)_xSiO_2(H_2O)_{0.61+1.39x}$ valid in the whole C/S range from 0.67 to 1.7 at H_2O saturation.

5. Discussion and conclusions

As shown in Section 3.1, the general Richardson and Groves' (RG) structural formula of C-S-H phases [19,27,33,72] can be converted into a sublattice solid solution model (Eq. (7)) having four kinds of structural sites (sublattices) with substituting chemical moieties or vacancies. Available structural and solubility data ([18] and refs. therein) suggest that substitutions in the BT (bridging tetrahedra) and IC (interlayer cation) sites are strongly interdependent. The addition of $Ca(OH)_2$ to the C-S-H–water system results in increased C/S ratio and decreased silicate chain length <CL> in C-S-H phase, and vice versa; this process is shown to be nearly reversible. In Section 4 of this contribution, this dependence was used for simplifying the sublattice solid solution model of C-S-H from 16 down to 3 or 4 end members (at H_2O saturation). Such SS models cover a realistic range of C-S-H compositions (0.67<C/S<1.5 or 1.8) and, even without introducing the non-ideality through excess Gibbs energy terms, provide a better description of C-S-H solubility than previous solid solution models.

In Section 3.1, it can be seen that the CSHQ SS model made of two 'tobermorite-like' and two 'jennite-like' end members with formulae referred to three tetrahedral sites (i.e. one dreierkette unit) suffers from somewhat unrealistic solubility curves in the interval 0.7<C/S<0.9 and over-predicts $[Si]_{AQ}$ at C/S>1.0. Hence, a relatively stable intermediate pentameric compound was assumed to exist in C-S-H with C/S≈1.0 (Section 3.2). On this basis, a simpler solid solution model for the defect-tobermorite C-S-H structure has been developed, in which the ordering was described using a sublattice model with two kinds of BTI sites, leading to an intermediate T5C end member. This 'basic' ternary CSH3T ideal model provides a surprisingly realistic description of the generic C-S-H solubility data (Fig. 3). Further on, the model was tuned up to yield a very good fit (Fig. 4) to the C″ curve solubility data [18] as well as <CL> NMR data for the set of C-S-H samples obtained by 'double decomposition', believed to produce mainly tobermorite-like C-S-H. The downscaled CSH3T model (Table 5) with simple ideal mixing produced the same curves. The quality of fit (Figs. 4 and 5) suggests that further improvement by introducing excess Gibbs energy terms such as those in (Eq. (13) in Ref. [71]) is not warranted.

The success of downscaling end members in the CSH3T SS model to reduce it to simple ideal mixing (where the activity of end member equals its mole fraction, $a_j = x_j$) suggested that the more general CSHQ SS model could also be improved by downscaling it to one tetrahedral site (see Table 6, Fig. 6). Indeed, this leads to a good fit to the C curve (C3S hydration C-S-H samples having largely jennite-like structure) experimental data [18] including the ^{29}Si NMR-measured <CL> values, which means that the downscaled CSHQ model still can be made consistent with the extent of silicate polymerization. As shown in a sensitivity study (see Appendix C), via the moderate adjustment of end member solubility products (within 0.3 to 0.6 pK units, see Table 6), this model can fit most of the published C-S-H solubility data sets and thus describe the behavior of many possible metastable C-S-H phases. Together with the molar volume and density variation (Table 7, Fig. 8) and temperature correction parameters (Table 8), the CSHQ SS model can be recommended for use in modeling cement hydration and reactive mass transport in cement-based materials.

Are there different C-S-H phases? Can they co-exist in one sample? On one hand, different solubility data sets (i.e. obtained using different preparation routes) may reflect a spectrum of metastable phases with structures ranging from purely tobermorite-like to largely jennite-like [18]. The CSHQ model can accommodate most of these differences by moderate adjustments of end member solubility products, thus leading to a collection of thermodynamically different (though similar in setup) C-S-H SS models. On the other hand, structural and spectroscopic investigations [22,34,36] reveal a pronounced structural transition around C/S = 1 in tobermorite-like C-S-H manifested e.g. in changes of the interlayer distance and of the Q parameter (<CL>). The success of CSH3T SS model suggests that such structural changes can be interpreted (on thermodynamic modeling side) as ordering effects, rather than as miscibility gaps caused by the co-existence of different phases like α- and β-C-S-H. The discontinuity between C/S = 1.5 and C/S = 1.8 at [Ca] = 0.022 M, interpreted in Ref. [30] as another invariant point of co-existence of β- and γ-C-S-H, cannot be reproduced in the CSH3T SS model (limited to C/S<1.5), but is covered by the CSHQ solid solution model.

In Fig. 9, C-S-H solubility curves modeled with GEM-Selektor code using CSHQ and CSH3T SS models are compared with the eye-guide curves C, C″ and A on the Jennings' diagram in [Ca]–[Si] space (see also Fig. 10 in Ref. [18]). As seen in Fig. 9, there is only qualitative agreement between the C curve and the CSHQ model curve, and between the C″ curve and the CSH3T model curve. However, both model trends are correct, and both solid solution models give even better descriptions of experimental data in [Ca]-C/S, [Si]-C/S and [<CL>]-C/S spaces than in the [Si]–[Ca] space (see Figs. 3–6). Keeping in mind that both SS models are rather simple, and that, in general, it is a difficult task to obtain equally good model fit in all coordinate spaces (see Fig. 1), the progress is remarkable, and the match between eye-guide curves C, C″ and the SS model curves appears reasonable. An open question remains, whether an SS model counterpart can be found for the A guideline curve in the range of [Ca] between 10 and 20 mM.

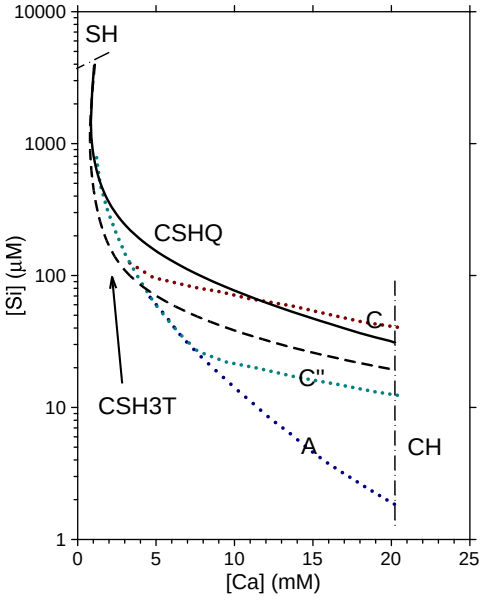

Fig. 9. Comparison of the downscaled CSHQ and CSH3T SS model curves (solid- and short-dashed, respectively) with the A (purely tobermorite-like C-S-H), C″ (mainly tobermorite-like C-S-H), and C (mainly jennite-like C-S-H) eye-guide curves (dotted) from Chen et al. [18] solubility diagram for metastable C-S-H phases. Thin dash-dot lines represent the appearance of stable portlandite (CH) and amorphous silica (SH) phases.

It is of interest to compare CSH3T and CSHQ SS models with sublattice-based models [55] and [56] (see also Section 2.3). Both quaternary SS models seem to be limited to H_2O saturation and consider two (independent) substitutions — $H_2SiO_4^{2-}$ for $H_2O_2^{2-}$ (or SiO_2 for vacancy) in BT sublattice sites, and Ca^{2+} for $2H^+$ (or CaO for H_2O) in IC (interlayer cation exchange) sites. Different to our present setup (with a combined substitution of Ca^{2+} plus H_2O for $2H^+ + SiO_2$ on BTI sites), both models have a fixed main tobermorite unit made of 2.33CaO and $2SiO_2$ (cf. $2CaSiO_{3.5}^-$ in our model derived from the RG structural model). As a consequence, the models [55,56] have a silica-rich end member with C/S = 0.77 which has more calcium than the 'protonated tobermorite' TobH end member (C/S = 0.67) used in the present study. To account for the solubility of C-S-H with C/S<0.77, another ternary solid solution involving amorphous SiO_2 end member was assumed to exist [56], equally unsupported with structural data as the binary CSH-I solid solution postulated in Ref. [10,54]. Whether all these complications really improve the quality of SS model fit to solubility data, remains questionable.

A comparison of (Fig. 5 in [56]) with Fig. 3,A for the CSH3T SS model shows nearly the same shape and similar position of the [Ca] curve in the solid C/S interval from 0.8 to 1.6. The quality of available solubility data at C/S<0.8 does not give any preference to the model [56] over a simple co-existence of pure SH and C-S-H phase with C/S = 0.68, as shown on Figs. 3, A,B or 5, A,B. Unfortunately, no model results in the [Ca]–[Si] space are presented in Ref. [56]. The model [55], especially with optimized non-ideality parameters, produces an excellent fit in [Ca]–[Si] space (see Fig. 4 in Ref. [55]), but it is not evident that the fit is equally good in [Ca]-C/S and [Si]-C/S spaces. The model [55] reproduces the typical dependence of *Q* parameter (or <CL>) on C/S ratio only in the strongly non-ideal case, whereas this dependence is built-in even in our ideal CSH3T model (see Fig. 5,D) and can be easily adjusted in the ideal CSHQ SS model (Fig. 6,C).

The reported advance in developing ideal sublattice SS models of C-S-H by simplifying the RG structural formulae, either with ordering around C/S = 1, or with downscaled jennite-like end members, poses two questions: (i) Is the usage of excess Gibbs energy parameters warranted at all for C-S-H phases? (ii) Might the high non-ideality in some published models be induced by an improper choice of end members?

The fact that good fits to the solubility data can be obtained with the ideal CSH3T or with the downscaled ideal CSHQ SS models can be understood in comparison with recent findings in thermodynamic solid-solution modeling of clays [73,74]. Mica-like dioctahedral clays (illites, smectites) are considered as solid solutions between muscovite $Si_3Al_3KO_{10}(OH)_2$ or paragonite $Si_3Al_3NaO_{10}(OH)_2$ and pyrophyllite $Si_4Al_2◊O_{10}(OH)_2$ (◊ stands for a vacancy), with variable interlayer H_2O contents. At elevated temperatures (50 to 200 °C), clays dehydrate, and the mixing between muscovite and pyrophyllite or between paragonite and pyrophyllite becomes strongly non-ideal, leading to miscibility gaps. However, as temperature decreases, intermediate compositions get stabilized by the incorporation of more and more interlayer water, until miscibility gaps disappear (see Fig. 10 in Ref. [73]; Fig. 1 in Ref. [74]).

This kind of stabilization by the interlayer H_2O leading to a 'near-ideal' mixing behavior in low-temperature fully-hydrated clay systems seems to be of broader importance, and should be expected to occur also in C-S-H systems and in LDH structures [76]. Conversely, as an answer to question (i), we may conclude that the inclusion of 'true' non-ideality parameters into CSHQ or CSH3T SS models is not warranted at least below *T* = 50 °C in fully-hydrated systems.

Concerning the question (ii), the answer is "probably yes". C-S-H end-member stoichiometries must retain certain degree of structural consistency including the silica chain length (<CL>) which cannot be less than two in the defect-tobermorite C-S-H. Hence, any end member having C/S>2.25 or silicon-free (such as portlandite Ca$(OH)_2$) cannot be feasible. Usage of such structurally incompatible end member can only be partially compensated by introducing a strong asymmetric non-ideality, which cannot be reconciled in terms of C-S-H structure and must be considered as an artifact. Any further complication of CSHQ or CSH3T SS models by introducing excess energy parameters is warranted only when a very accurate and extensive experimental data set in the whole range 0.6<C/S<1.7 becomes available, but such data set does not exist so far.

One possible objection to the present formulation of CSHQ and CSH3T SS models could be that some species substituting in sublattice sites have fractional element stoichiometry coefficients (see Table 3, also Appendix A). This is legal in macroscopic chemical thermodynamic models (where any stoichiometry coefficient is just the ratio of mole amounts), but may be invalid in atomistic models that cannot operate with ½ of Ca ion or of ½ of Si atom (or any non-integer fraction). So, to develop a fully atomistically-consistent solid solution model, one should avoid using fractional stoichiometries of species substituted on sublattice sites, or avoid any end-member downscaling that implies such fractional stoichiometries.

Keeping this objection in mind, the CHS3T and CSHQ SS models of fully-hydrated C-S-H suggested in this contribution, are not yet '100% structurally consistent', even though they appear much more 'structurally consistent' than previous simple binary SS models [10,13,14,75], at least with respect to mean <CL> values as function of C/S. This is about the same level of atomistic (structural) consistency as that in the RG structural model (cf. [19,20]) or in the Thomas and Jennings SS model [55]. In the latter, a somewhat different 'sublattice formalism' has been applied, albeit with a fractional stoichiometry $(:CaO:)_{2.33}$ in the first sub-lattice.

However, there is not much sense to re-define sublattice-based C-S-H solid solution models at present because of an on-going work on producing more experimental data for C-S-H solubility/stability in presence of Al, Na and K, at the same time elucidating their structural location and environment in the interlayer (together with Ca ions) with spectroscopic studies and advanced molecular modeling. Completion of these projects will certainly allow constructing more structurally consistent *and* atomistically feasible SS models of C-S-H, also capable of reproducing the effects of incorporation of aluminate and alkali ions, of short- and long-range ordering, and of (variable) hydration. Due to many more end members and possible need to involve the non-ideality, such SS models will be possible to compute only using GEM thermodynamic equilibrium solvers, and to parameterize using advanced fitting algorithms.

Nevertheless, the CSHQ and CSH3T SS models of C-S-H appear to be useful at present at least for three reasons. Firstly, they are still relatively simple and (in downscaled form) can be computed not only in GEM, but also in MAL codes such as PHREEQC ([62]; E. Martens, pers. comm.). Secondly, compared with the previous ideal SS models, both CSHQ and CSH3T yield a more accurate description of C-S-H solubility (also in [Ca]–[Si] coordinates), as well as of H_2O content and density in fully hydrated systems; only one SS phase (either CSHQ or CSH3T) needs to be included into the system, instead of two SS phases before. Thirdly, the extension with minor cations is rather straightforward for the CSH3T SS model, if structural sites occupied with a cation are known from the spectroscopic evidence. Such recent work, aimed at modeling U^{VI} incorporation into C-S-H, resulted in a good description of experimental data with a CSH3T-U SS model extended with three U-containing end members [77].

Further progress in modeling stability and solubility of C-S-H phases is possible by combining the sublattice solid solution tobermorite-like core with the ion exchange, surface complexation, and surface precipitation on outer particle surfaces of C-S-H.

Acknowledgments

Thanks to Urs Berner, Xavier Gaona, Michael Kersten, Barbara Lothenbach, Jan Tits and Erich Wieland for stimulating discussions, to

Urs Berner for the provision of the digitized C-S-H solubility data, and to X. Gaona for help with Fig. 2. Partial financial support from Nagra (Wettingen, Switzerland) is gratefully acknowledged.

Appendix A. Derivation of stoichometries of end members in sublattice CSHQ SS models

Combining one species per sublattice site from Table A.1 would result in a list of 16 end-member formulae. Such a solid solution model appears to be far too complex and too difficult to parameterize, especially when substitutions in different sublattices are not independent.

An obvious first step is to fix the H_2O occupancy in IW sites to 4/5 (in saturated state), or to set the IW site ratio to 4 with unity H_2O occupancy, which reduces the SS model to 8 end members (Table A.2). This 'simplified' sublattice model would exactly cover the composition and silicate chain length fields shown in solid lines on the RG diagram (see Fig. 25 in Ref. [19]), but it is perhaps still too complex to be useful in thermodynamic calculations. Fortunately, the structural and solubility data (Sections 2.1 and 2.2) let the SS model be simplified further.

There is an emerging agreement in that the minimal C/S ratio in aged C-S-H phases is about 2/3 [18,19,22,36], and such C-S-H has the longest mean silicate chain length <CL>. Hence, the polymeric TH end member (with C/S = 2/3) must be considered as sufficiently stable. Interestingly, both TC and T2H end members have C/S = 1, but differ in CL and *u* values (see Table A.2). However, the transition from TC to T2H end member (i.e. depolymerization with simultaneous increase in protonation of silanol sites) contradicts the generally observed trend of *decreasing* <CL> with increasing Ca content [18] mainly below C/S = 1.1. Thus, the TC end member must be much less stable than the T2H end member.

Table A.1
C-S-H sublattice scheme derived from the RG structural model [19], see Eq. (7).

C-S-H sublattice			Species	RG model freedom	Comment
Index	Site	Ratio			
0	IC	2	H^+, $½Ca^{2+}$, …	*u*	Interlayer cation exchange sites
1	TU	2	$CaSiO_{3.5}^-$	fixed	Main tobermorite layer unit
2	BT	1	SiO_2, V_{BT}, …	*v*	Bridging tetrahedral site
3	CU	2	$Ca(OH)_2$,V_{CU}, …	*y*, *u*	Optional J or CH extra-Ca unit
4	IW	5	H_2O, V_{IW}	*m*	Interlayer non-hydroxyl water sites

V_{BT}, V_{CU}, V_{IW} denote vacancies in the respective sites; J stands for 'jennite-like'.

Table A.2
A subset of end members in C-S-H sublattice model with fixed IW site occupancy.

End member				Structural formula	CL	Bulk formula (per 1 Si)
ID	*u*	*v*	*y*			
TH	2	0	0	$[H^+]_2$:$[CaSiO_{3.5}^-]_2$:$[SiO_2]_1$:$[V_{CU}]_2$:$[H_2O]_4$	∞	$(CaO)_{2/3}SiO_2(H_2O)_{5/3}$
TC	0	0	2	$[1/2Ca^+]_2$:$[CaSiO_{3.5}^-]_2$:$[SiO_2]_1$:$[V_{CU}]_2$:$[H_2O]_4$	∞	$(CaO)_1SiO_2(H_2O)_{4/3}$
T2H	2	1	0	$[H^+]_2$:$[CaSiO_{3.5}^-]_2$:$[V_{BT}]_1$:$[V_{CU}]_2$:$[H_2O]_4$	2	$(CaO)_1SiO_2(H_2O)_{5/2}$
T2C	0	1	2	$[1/2Ca^+]_2$:$[CaSiO_{3.5}^-]_2$:$[V_{BT}]_1$:$[V_{CU}]_2$:$[H_2O]_4$	2	$(CaO)_{3/2}SiO_2(H_2O)_{4/2}$
JH	2	0	4	$[H^+]_2$:$[CaSiO_{3.5}^-]_2$:$[SiO_2]_1$:$[Ca(OH)_2]_2$:$[H_2O]_4$	∞	$(CaO)_{4/3}SiO_2(H_2O)_{7/3}$
JC	0	0	6	$[1/2Ca^+]_2$:$[CaSiO_{3.5}^-]_2$:$[SiO_2]_1$:$[Ca(OH)_2]_2$:$[H_2O]_4$	∞	$(CaO)_{5/3}SiO_2(H_2O)_{6/3}$
J2H	2	1	4	$[H^+]_2$:$[CaSiO_{3.5}^-]_2$:$[V_{BT}]_1$:$[Ca(OH)_2]_2$:$[H_2O]_4$	2	$(CaO)_2SiO_2(H_2O)_{7/2}$
J2C	0	1	6	$[1/2Ca^+]_2$:$[CaSiO_{3.5}^-]_2$:$[V_{BT}]_1$:$[Ca(OH)_2]_2$:$[H_2O]_4$	2	$(CaO)_{5/2}SiO_2(H_2O)_{6/2}$

CL stands for the silicate chain length; *u*,*v*,*y* are parameters of the rescaled RG model (see text).

Moreover, the full occupation of IC sites with Ca^{2+} ions may be energetically less favorable than the partial occupation (implicit in Taylor's TJ model with $u = 1$ and $y = 1$). If so, the end-point in tobermorite-type C-S-H with dimeric structure should be between C/S = 5/4 [22] and C/S = 6/4. Some excess Ca^{2+} may also be bound on the outer surfaces of C-S-H nanoparticles (see Eq. (4) in Ref. [30]).

The C-S-H SS model can be reduced to four end members by taking into account an inverse dependence of <CL> and Ca content in C-S-H as demonstrated by Chen et al. [18], which can also be viewed as a pronounced short-range ordering. This reduction can be done either by introducing a strong non-ideal interaction between IC and BT sites (as done in Ref. [55]), or by coupling BT and IC substitutions on a combined BTI sublattice site:

$$\left[BTI^+\right]_2: [TU^-]_2: \left[CU^0\right]_2: \left[IW^0\right]_4. \tag{A.1}$$

This reduces the number of end members from 8 to 4, provided that plausible $2H^+/Ca^{2+}$ ratios in end members are chosen, and the vacancy in BT site is replaced by an H_2O molecule. Table A.3 contains the resulting sublattice scheme of $[A,B]_2[C,D]_2X$ type, and Table A.4 lists its four end members, assuming complete BTI H^+ occupancy in TobH, JenH and complete BTI Ca^{2+} occupancy in T2C, J2C end members. In the following, this kind of solid solution model will be termed CSHQ (the C-S-H quaternary model).

Between four CSHQ end members, a reciprocal reaction can be written:

$$\text{JenH} + \text{T2C} = \text{TobH} + \text{J2C} \tag{A.2}$$

with the molar Gibbs energy effect

$$\Delta G_{\text{rcp}} = G^{\text{o}}_{f\text{TobH}} + G^{\text{o}}_{f\text{J2C}} - G^{\text{o}}_{f\text{JenH}} - G^{\text{o}}_{f\text{T2C}} \tag{A.3}$$

The usual initial assumption is $\Delta G_{\text{rcp}} = 0$.

For the CSHQ model (Table A.4, Eqs. (9)–(15)), a reasonable description of a generic solubility data set combined from sources [18,39–41,43–45] has been obtained in trial GEM-Selektor calculations with parameters given in Table A.5. The "best" visual fit is similar to that of the C-S-H ideal SS model from Cemdata'07 database (see Fig. 1), i.e. relatively good for $[Ca]_{AQ}$ with over-prediction of $[Si]_{AQ}$ at C/S > 1.0. Inspection of calculated composition of the CSHQ phase showed that

Table A.3
A simplified CSHQ sublattice scheme with coupled BTI sites.

C-S-H sublattice			Species	RG freedom	Comment
Index	Site	Ratio			
0	BTI	2	$Si_{0.5}OH^+$, $HO_{0.5}Ca_{0.5}^+$	$u/2 + v = 1$	BT-Interlayer cation sites
1	TU	2	$CaSiO_{3.5}^-$	fixed	Main tobermorite unit
2	CU	2	$Ca(OH)_2$,V_{CU}, …	*y*, *u*	Optional J or CH extra-Ca unit
3	IW	4	H_2O	fixed	Interlayer water sites

Table A.4
End members of the CSHQ solid solution model with coupled BTI sublattice.

End member				Sublattice formula	CL	Bulk formula
ID	*u*	*v*	*y*			
TobH	2	0	0	$[Si_{0.5}OH^+]_2$:$[CaSiO_{3.5}^-]_2$:$[V_{CU}]_2$:$[H_2O]_4$	∞	$[(CaO)_{2/3}SiO_2(H_2O)_{5/3}]_3$
T2C	0	1	2	$[HO_{0.5}Ca_{0.5}^+]_2$:$[CaSiO_{3.5}^-]_2$:$[V_{CU}]_2$:$[H_2O]_4$	2	$[(CaO)_{3/2}SiO_2(H_2O)_{5/2}]_2$
JenH	2	0	4	$[Si_{0.5}OH^+]_2$:$[CaSiO_{3.5}^-]_2$:$[Ca(OH)_2]_2$:$[H_2O]_4$	∞	$[(CaO)_{4/3}SiO_2(H_2O)_{7/3}]_3$
J2C	0	1	6	$[HO_{0.5}Ca_{0.5}^+]_2$:$[CaSiO_{3.5}^-]_2$:$[Ca(OH)_2]_2$:$[H_2O]_4$	2	$[(CaO)_{5/2}SiO_2(H_2O)_{7/2}]_2$

Table A.5
Parameters adjusted for the CSHQ model (Table A.4) in trial GEM-Selektor calculations; $\Delta G_{rcp} = 30.14$ kJ mol^{-1}.

End member	Bulk formula (per dreierkette)	G^o_f kJ mol^{-1}	$\mathrm{Log}_{10}K$
TobH	$(CaO)_2(SiO_2)_3(H_2O)_5$	−5124.21	−12.60
T2C	$(CaO)_3(SiO_2)_2(H_2O)_5$	−4926.86	−11.15
JenH	$(CaO)_4(SiO_2)_3(H_2O)_7$	−6941.81	−16.73
J2C	$(CaO)_5(SiO_2)_2(H_2O)_7$	−6714.32	−10.00

$\log_{10}K$ is given for the reaction $(CaO)_x(SiO_2)_y(H_2O)_z = ySiO_2{,}am + xCa(OH)_2{,}cr + (z-x)H_2O{,}aq$.

'dimeric' end members T2C and J2C were minor in the whole C/S interval. This contradicts the ^{29}Si NMR <CL> data (e.g. [18]) that suggest that these end members should prevail at C/S > 1.1. Hence, this solid solution model is not yet structurally realistic.

As seen on Fig. A.1, the [Si] and [Ca] curves cross at C/S < 0.7, whereas the majority of experimental data suggest the congruence point at 0.8 < C/S < 0.9. Note also that neglecting the fictive activity coefficients (Eqs. (15a)–(15d)) results in a large vertical step in solubility curves at 1.33 < C/S < 1.5 and renders the model fit completely unsatisfactory (not shown).

Further, the CSHQ SS model (Table A.4, Eqs. (15a)–(15d), Table A.5) has been compared with another model variant expressed with the sublattice formula

$$\left[BTI^{2+}\right]_1 : [TU^-]_2 : \left[CU^0\right]_2 : \left[IW^0\right]_4$$

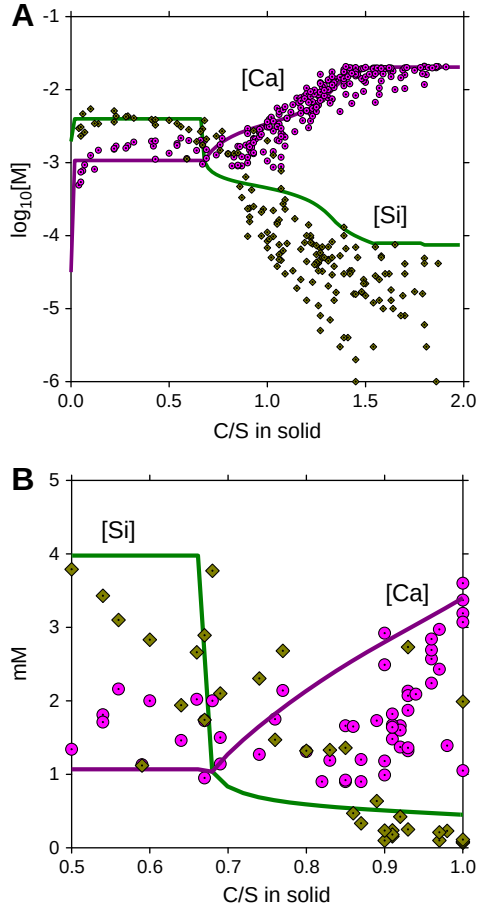

Fig. A.1. The CSHQ aqueous – solid solution model (Tables A.4, A.5), shown as continuous curves against C/S – the bulk mole Ca/Si ratio in the solid part of the system. Circles [Ca] and diamonds [Si] are the C-S-H aqueous solubility data from [18,39–41,43–45]. (B) is a fragment of the solubility diagram (A) taken in the linear molarity scale (millimolar).

Table A.6
End members in the alternative CSHQ SS model with coupled BTI sublattice.

End member				Sublattice formula	CL	Bulk formula
ID	u	v	y			
TobH	2	0	0	$[Si_{0.5}OH^+]_2$:$[CaSiO_{3.5}^-]_2$:$[V_{CU}]_2$:$[H_2O]_{7/2}$	∞	$[(CaO)_{2/3}SiO_2(H_2O)_{9/6}]_3$
T2	1	1	1	$[H_{1.5}O_{0.5}Ca_{0.25}^+]_2$:$[CaSiO_{3.5}^-]_2$:$[V_{CU}]_2$:$[H_2O]_4$	2	$[(CaO)_{5/4}SiO_2(H_2O)_{11/4}]_2$
JenH	2	0	4	$[Si_{0.5}OH^+]_2$:$[CaSiO_{3.5}^-]_2$:$[Ca(OH)_2]_2$:$[H_2O]_{7/2}$	∞	$[(CaO)_{4/3}SiO_2(H_2O)_{13/6}]_3$
J2	1	1	5	$[H_{1.5}O_{0.5}Ca_{0.25}^+]_2$:$[CaSiO_{3.5}^-]_2$:$[Ca(OH)_2]_2$:$[H_2O]_4$	2	$[(CaO)_{9/4}SiO_2(H_2O)_{15/4}]_2$

with one BTI site where one H_2OCa^{2+} species is substituted with one $SiO_2H_2^{2+}$ species. Accordingly, structural formulae in Table A.4 change to e.g. $[H_2SiO_2^{+2}]_1$:$[CaSiO_{3.5}^-]_2$:$[V_{CU}]_2$:$[H_2O]_4$ etc., and Eqs. (14), (15) to

$$\mu_{TobH} = G^o_{TobH} - y_{Ca,BTI}y_{CH,CU}\Delta G_{rcp} + RT(\ln y_{Si,BTI} + 2\ln y_{Vcu,CU})$$

$$\ln\lambda_{TobH} = \ln y_{Si,BTI} + 2\ln y_{Vcu,CU} - y_{Ca,BTI}y_{CH,CU}\frac{\Delta G_{rcp}}{RT} - \ln x_{TobH}$$

and so on. We found that this second variant fits the solubility data even worse than the first one (not shown).

The nanocrystalline C-S-H(I) phase with purely tobermorite structure exists in the compositional space between ordered compounds with C/S = 0.67 (fully polymerized TobH) and 1.25 (dimeric half-protonated tobermorite T2) [22,26,37,69]. Assuming the existence of a similar series from the fully polymerized jennite JenH to dimeric half-protonated jennite J2, an alternative CSHQ model can be built, as shown in Table A.6. In the implementation of this SS model, Eqs. (9)–(15) apply after renaming the subscripts T2C to T2 and J2C to J2. This alternative model will be further used in the main text in deriving the downscaled simple ideal CSHQ model.

Non-hydroxyl H_2O content per dreierkette unit in TobH was set here to $3^1/_2$ and that in T2 to 4 similar to [22]. Non-hydroxyl water content in JenH was calculated from the reciprocal reaction TobH + J2 = T2 + JenH, assuming the same non-hydroxyl H_2O content in J2 as in T2 end members.

Appendix B

Phases, components, and thermodynamic data in the CaO–SiO_2–H_2O–N_2 system at $P = 1$ bar, T = 298.15 K (except C-S-H solid solution phases).

Table B.1
Standard partial molal Gibbs energy and volume of aqueous species used in GEM-Selektor calculations (from GEMS version of Nagra-PSI database [64]).

Aqueous species	G^o_f, kJ mol^{-1}	V^o, cm^3 mol^{-1}
Ca^{+2}	−552.790	−18.439
$Ca(OH)^+$	−717.024	5.7625
$Ca(HSiO_3)^+$	−1574.238	−6.7366
$Ca(SiO_3)^0$	−1517.557	15.693
$HSiO_3^-$	−1014.598	4.5259
SiO_2^0	−833.411	16.061
SiO_3^{-2}	−938.510	34.132
H_2^0	17.729	25.264
N_2^0	18.194	33.407
O_2^0	16.446	30.501
OH^-	−157.270	−4.7078
H^+	0	0

Table B.2
Standard molar properties of water and solids (from GEMS Nagra-PSI database) used in GEM-Selektor calculations and in deriving thermodynamic properties listed in Table 8.

Phase	Component	V^o, cm^3 mol^{-1}	G^o_f, kJ mol^{-1}	H^o, kJ mol^{-1}	S^o, J K^{-1} mol^{-1}	Cp^o, J K^{-1} mol^{-1}
Aqueous	Water H_2O	18.0684	−237.18	−285.88	69.92	75.36
CH	Portlandite $Ca(OH)_2$	33.06	−897.01	−984.68	83.40	87.51
SH	Amorphous silica SiO_2	29.00	−848.90	−903.45	41.00	44.43

Note: Ideal gas mixture of H_2, N_2, O_2 has also been used in GEM-Selektor calculations.

Appendix C. Supplementary data

Supplementary information file to this article can be found online at doi:10.1016/j.cemconres.2011.01.012.

References

[1] H.F.W. Taylor, Cement Chemistry, Academic Press, London, 1990.
[2] N.D.M. Evans, Binding mechanisms of radionuclides to cement, Cement and Concrete Research 38 (2008) 543–553.
[3] J. Tits, T. Stumpf, T. Rabung, E. Wieland, T. Fanghänel, Uptake of Cm(III) and Eu(III) by calcium silicate hydrates: A solution chemistry and time-resolved laser fluorescence spectroscopy study, Environmental Science and Technology 37 (2003) 3568–3573.
[4] J. Tits, E. Wieland, C.J. Müller, C. Landesman, M.H. Bradbury, Strontium binding by calcium silicate hydrates, J. Colloid Interface Sci. 300 (2006) 78–87.
[5] J. Tits, K. Iijima, E. Wieland, G. Kamei, The uptake of radium by calcium silicate hydrates and hardened cement paste, Radiochimica Acta 94 (2006) 637–643.
[6] F. Ziegler, R. Giere, C.A. Johnson, Sorption mechanisms of zinc to calcium silicate hydrate: Sorption and microscopic investigations, Environmental Science and Technology 35 (2001) 4556–4561.
[7] H.F.W. Taylor, Studies on the chemistry and microstructure of cement pastes, in: F. P. Glasser (Ed.), The Chemistry and Chemically-Related Properties of Cement, vol. 35, 1984, pp. 65–82, London.
[8] K. Fujii, W. Kondo, Estimation of thermochemical data for calcium silicate hydrate (C-S-H), Journal of American Ceramic Society 66 (1983) C-220–C-221.
[9] H.J.H. Brouwers, The work of Powers and Brownyard revisited: Part 1, Cement and Concrete Research 34 (2004) 1697–1716.
[10] D.A. Kulik, M. Kersten, Aqueous solubility diagrams for cementitious waste stabilization systems: II, End-member stoichiometries of ideal calcium silicate hydrate solid solutions, Journal of the American Ceramic Society 84 (2001) 3017–3026.
[11] B. Lothenbach, F. Winnefeld, Thermodynamic modelling of the hydration of Portland cement, Cement and Concrete Research 36 (2006) 209–226.
[12] B. Lothenbach, E. Wieland, A thermodynamic approach to the hydration of sulphate-resisting Portland cement, Waste Management 26 (2006) 706–719.
[13] B. Lothenbach, T. Matschei, G. Möschner, F.P. Glasser, Thermodynamic modelling of the effect of temperature on the hydration and porosity of Portland cement, Cement and Concrete Research 38 (2008) 1–18.
[14] T. Matschei, B. Lothenbach, F.P. Glasser, Thermodynamic properties of Portland cement hydrates in the system $CaO–Al_2O_3–SiO_2–CaSO_4–CaCO_3–H_2O$, Cement and Concrete Research 37 (2007) 1379–1410.
[15] F. Brunet, P. Bertani, T. Charpentier, A. Nonat, J. Virlet, Application of ^{29}Si Homonuclear and $^{1}H–^{29}Si$ Heteronuclear NMR Correlation to Structural Studies of Calcium Silicate Hydrates, Journal of Physical Chemistry B 108 (2004) 15494–15502.
[16] E. Bonaccorsi, S. Merlino, H.F.W. Taylor, The crystal structure of jennite, $Ca_9Si_6O_{18}(OH)_6\times 8H_2O$, Cement and Concrete Research 34 (2004) 1481–1488.
[17] E. Bonaccorsi, S. Merlino, A.R. Kampf, The crystal structure of Tobermorite 14A (Plombierite), a C-S-H phase, Journal of the American Ceramic Society 88 (2005) 505–512.
[18] J.J. Chen, J.J. Thomas, H.F.W. Taylor, H.M. Jennings, Solubility and structure of calcium silicate hydrate, Cement and Concrete Research 34 (2004) 1499–1519.
[19] I.G. Richardson, Tobermorite/jennite- and tobermorite/calcium hydroxide-based models for the structure of C-S-H: applicability to hardened pastes of tricalcium silicate, h-dicalcium silicate, Portland cement, and blends of Portland cement with blast-furnace slag, metakaolin, or silica fume, Cement and Concrete Research 34 (2004) 1733–1777.
[20] I.G. Richardson, The calcium silicate hydrates, Cement and Concrete Research 38 (2008) 137–158.
[21] K. Garbev, P. Stemmermann, L. Black, C. Breen, J. Yarwood, B. Gasharova, Structural features of C-S-H(I) and its carbonation in air — a Raman spectroscopic study. Part I: Fresh phases, Journal of the American Ceramic Society 90 (2007) 900–907.
[22] K. Garbev, M. Bornefeld, G. Beuchle, P. Stemmermann, Cell dimensions and composition of nanocrystalline calcium silicate hydrate solid solutions. Part 2: X-ray and thermogravimetry study, J. American Ceramic Society 91 (2008) 3015–3023.
[23] J. Skibsted, C. Hall, Characterization of cement minerals, cements and their reaction products at the atomic and nano scale, Cement and Concrete Research 38 (2008) 205–225.
[24] H.F.W. Taylor, A discussion on the papers "Models for the composition and structure of calcium silicate hydrate (C-S-H) gel in hardened thrcalcium silicate pastes" and "The incorporation of minor and trace elements into calcium silicate hydrate (C-S-H) gel in hardened cement pastes" by I.G.Richardson and G.W. Groves, Cement and Concrete Research 23 (1993) 995–998.
[25] H.F.W. Taylor, Tobermorite, jennite, and cement gel, Zeitschrift für Kristallographie 202 (1992) 41–50.
[26] H.F.W. Taylor, Proposed structure for calcium silicate hydrate gel, Journal of the American Ceramic Society 69 (1986) 464–467.
[27] I.G. Richardson, G.W. Groves, Models for the composition and structure of calcium silicate hydrate (C-S-H) gel in hardened tricalcium silicate pastes, Cement and Concrete Research 22 (1992) 1001–1010.
[28] X. Cong, R.J. Kirkpatrick, ^{29}Si MAS NMR study of the structure of calcium silicate hydrate, Advances in Cement Based Materials 3 (1996) 144–156.
[29] X. Cong, R.J. Kirkpatrick, ^{29}Si and ^{17}O NMR investigation of the structure of some crystalline calcium silicate hydrates, Advances in Cement Based Materials 3 (1996) 133–143.
[30] A. Nonat, The structure and stoichiometry of C-S-H, Cement and Concrete Research 34 (2004) 1521–1528.
[31] C. Labbez, A. Nonat, I. Pochard, B. Joensson, Experimental and theoretical evidence of overcharging of calcium silicate hydrate, Journal of Colloid and Interface Science 309 (2007) 303–307.
[32] B. Joensson, A. Nonat, C. Labbez, B. Cabane, H. Wennerstroem, Controlling the cohesion of cement paste, Langmuir 21 (2005) 9211–9221.
[33] I.G. Richardson, G.W. Groves, The incorporation of minor and trace elements into calcium silicate hydrate (C-S-H) gel in hardened cement pastes, Cement and Concrete Research 23 (1993) 131–138.
[34] A. Nonat, X. Lecoq, The structure, stoichiometry and properties of C-S-H prepared by C3S hydration under controlled conditions, in: P. Grimmer, A.-R. Grimmer, H. Zanni, P. Sozzani (Eds.), Nuclear Magnetic Resonance Spectroscopy of Cement-Based Materials, Springer, Berlin, 1998, pp. 197–207.
[35] H. Stade, D. Müller, On the coordination of Al in ill-crystallized C-S-H phases formed by hydration of tricalcium silicate and by precipitation reactions at ambient temperature, Cement and Concrete Research 17 (1987) 553–561.
[36] K. Garbev, G. Beuchle, M. Bornefeld, L. Black, P. Stemmermann, Cell dimensions and composition of nanocrystalline calcium silicate hydrate solid solutions. Part 1: Synchrotron-based X-ray diffraction, Journal of the American Ceramic Society 91 (2008) 3005–3014.
[37] H. Stade, W. Wieker, Zum Aufbau schlecht geordneter Calciumhydrogensilikate. I. Bildung und Eigenschaften einer schlecht geordneten Calciumhydrogensilikat-phase Zeitschrift für, Anorganische und Allgemeine Chemie 466 (1980) 55–70.
[38] H.M. Jennings, Refinements to colloid model of C-S-H in cement: CM-II, Cement and Concrete Research 38 (2008) 275–289.
[39] K. Fujii, W. Kondo, Heterogeneous equilibrium of calcium silicate hydrate in water at 30 °C. Journal Chemical Society Dalton Transactions 2 (1981) 645–651.
[40] E.P. Flint, L.S. Wells, Study of the system $CaO–SiO_2–H2O$ at 30° C and of the reaction of water on the anhydrous calcium silicates, Bureau of Standards Journal of Research 12 (1934) 751–783.
[41] S.A. Greenberg, T.N. Chang, Investigation of the colloidal hydrated calcium silicates. II. Solubility relationships in the calcium oxide–silica–water system at 25°, Journal of Physical Chemistry 69 (1965) 182–188.
[42] G.L. Kalousek, Studies of portions of the quaternary system soda–lime–silica–water at 25 C, Journal of Research, National Bureau of Standards 32 (1944) 285–302.
[43] G.L. Kalousek, Application of differential thermal analysis in a study of the system lime–silica–water, 3rd International Symposium on Cement Chemistry, Cement and Concrete Association, London, 1952, pp. 296–311.
[44] P.S. Roller, G.J. Ervin, The system calcium oxide–silica–water at 30°. The association of silicate ion in dilute alkaline solution, Journal of the American Chemical Society 62 (1940) 461–471.
[45] H.F.W. Taylor, Hydrated calcium silicates. Part I. Compound formation at ordinary temperatures, Journal of the Chemical Society of London 276 (1950) 3682–3690.
[46] C.S. Walker, D. Savage, M. Tyrer, K.V. Ragnarsdottir, Non-ideal solid solution aqueous solution modeling of synthetic calcium silicate hydrate, Cement and Concrete Research 37 (2007) 502–511.
[47] A.-C. Courault, Simulation experimentale des C-S-H dans les betons modernes: Etude de la composition et de proprietes a l'equilibre dans des milieux complexes, vol. PhD, Universite de Bourgogne, Dijon, 2000, p. 203.
[48] D. Sugiyama, T. Fujita, A thermodynamic model of dissolution and precipitation of calcium silicate hydrates, Cement and Concrete Research 36 (2006) 227–237.
[49] U.R. Berner, Modelling the incongruent dissolution of hydrated cement minerals, Radiochimica Acta 44/45 (1988) 387–393.
[50] U.R. Berner, Evolution of pore water chemistry during degradation of cement in a radioactive waste repository environment, Waste Management 12 (1992) 201–219.
[51] H.M. Jennings, Aqueous solubility relationships for two types of calcium silicate hydrate, Journal of the American Ceramic Society 69 (1986) 614–618.
[52] P. Lu, G. Sun, J.F. Young, Phase composition of hydrated DSP cement paste, Journal of the American Ceramic Society 76 (1993) 1003–1007.
[53] E.J. Reardon, Problems and approaches to the prediction of the chemical composition in cement/water systems, Waste Management 12 (1992) 221–239.
[54] V.A. Sinitsyn, D.A. Kulik, M.S. Khodorivsky, I.K. Karpov, Prediction of solid-aqueous equilibria in cementitious systems using Gibbs energy minimization: I.Multiphase aqueous-ideal solid solution models, MRS Symposia Proceedings 506 (1998) 953–960.

[55] J.J. Thomas, H.M. Jennings, Free-energy-based model of chemical equilibria in the $CaO–SiO_2–H_2O$ System, Journal of the American Ceramic Society 81 (1998) 606–612.
[56] J.A. Gisby, R.H. Davies, A.T. Dinsdale, M. Tyrer, F.P. Glasser, J. Hill, P. Livesey, C. Walker, C-S-H solubility modeling at different temperatures, in: J.J. Beaudoin, J.M. Makar, L. Raki (Eds.), 12th International Congress on the Chemistry of Cement, Cement Association of Canada, Montreal, Canada, 2007, p. 12,, W1-05.4.
[57] H.L. Lukas, S. Fries, B. Sundman, Computational Thermodynamics: The Calphad Method, Cambridge University Press, Cambridge, 2007.
[58] J. Bruno, D. Bosbach, D. Kulik, A. Navrotsky, Chemical thermodynamics of solid solutions of interest in radioactive waste management, A state-of-the-art report, OECD NEA, Paris, 2007.
[59] M.M. Rahman, S. Nagasaki, S. Tanaka, A model for dissolution of $CaO–SiO_2–H_2O$ gel at Ca/Si>1, Cement and Concrete Research 29 (1999) 1091–1097.
[60] M. Kersten, Aqueous solubility diagrams for cementitious waste stabilization systems. 1. The C-S-H solid–solution system, Environmental and Science Technology 30 (1996) 2286–2293.
[61] S. Boerjesson, A. Emren, C. Ekberg, A thermodynamic model for the calcium silicate hydrate gel, modelled as a non-ideal binary solid solution, Cement and Concrete Research 27 (1997) 1649–1657.
[62] E. Martens, D. Jacques, T. Van Gerven, L. Wang, D. Mallants, Geochemical modeling of leaching of Ca, Mg, Al, and Pb from cementitious waste forms, Cement and Concrete Research 40 (2010) 1298–1305.
[63] W.A. Oates, Ideal solutions, Journal of Chemical Education 46 (1969) 501–504.
[64] W. Hummel, U.R. Berner, E. Curti, F.J. Pearson Jr., T. Thoenen, Nagra/PSI Chemical Thermodynamic Data Base 01/01, Radiochimica Acta 90 (2002) 805–813.
[65] M. Hillert, Phase Equilibria, Phase Diagrams and Phase Transformations: Their Thermodynamic Basis, Cambridge University Press, Cambridge, 1998.
[66] C.A. Geiger (Ed.), Solid Solutions in Silicate and Oxide Systems of Geological Importance, Eötvös University Press, Budapest, 2001.
[67] I.K. Karpov, K.V. Chudnenko, D.A. Kulik, Modeling chemical mass-transfer in geochemical processes: Thermodynamic relations, conditions of equilibria and numerical algorithms, American Journal of Science 297 (1997) 767–806.
[68] D.L. Parkhurst, C.A.J. Appelo, User's guide to PHREEQC (version 2) — a computer program for speciation, batch-reaction, one-dimensional transport, and inverse geochemical calculations, U.S.G.S. Water-Resources Investigations Report 99–4259, 1999, p. 312, Denver, Colorado.
[69] H. Stade, Zum Aufbau schlecht geordneter Calciumhydrogensilikate. II. Eine Phase bestehend aus Poly- und Disilikate, Zeitschrift für, Anorganische und Allgemeine Chemie 470 (1980) 69–83.
[70] W. Hummel, U.R. Berner, E. Curti, F.J. Pearson Jr, T. Thoenen, Nagra-PSI chemical thermodynamic database, version 01/01, Universal Publishers/Upubl.com, New York, 2002.
[71] T. Holland, R. Powell, Activity–composition relations for phases in petrological calculations: an asymmetric multicomponent formulation, Contributions to Mineralogy and Petrology 145 (2003) 492–501.
[72] I.G. Richardson, G.W. Groves, A reply to discussions by H.F.W. Taylor of the papers "Models for the composition and structure of calcium silicate hydrate (C-S-H) gel in hardened thrcalcium silicate pastes" and "The incorporation of minor and trace elements into calcium silicate hydrate (C-S-H) gel in hardened cement pastes" by I.G. Richardson and G.W.Groves, Cement and Concrete Research 23 (1993) 999–1000.
[73] O. Vidal, B. Dubacq, Thermodynamic modelling of clay dehydration, stability and compositional evolution with temperature, pressure and H_2O activity, Geochimica et Cosmochimica Acta 73 (2009) 6544–6564.
[74] B. Dubacq, O. Vidal, V. De Andrade, Dehydration of dioctahedral aluminous phyllosilicates: thermodynamic modelling and implications for thermobarometric estimates, Contributions to Mineralogy and Petrology 159 (2010) 159–174.
[75] D.A. Kulik, M. Kersten, Aqueous solubility diagrams for cementitious waste stabilization systems. 4. A carbonation model for Zn-doped calcium silicate hydrate by Gibbs energy minimization, Environmental Science and Technology 36 (2002) 2926–2931.
[76] X. Gaona, D.A. Kulik, N. Macé, E. Wieland, Aqueous-solid solution thermodynamic model of U(VI) uptake in C-S-H phases (2011), Applied Geochemistry, in submission.
[77] K.B. Rozov, U. Berner, D.A. Kulik, L. Diamond, Solubility and thermodynamic properties of hydrotalcite–pyroaurite carbonate-containing solid solutions with 3:1 Mg/(Al + Fe) ratio (2011), Chemical Geology, in submission.